



## Supporting Information for

### A lever hypothesis for Synaptotagmin-1 action in neurotransmitter release

Kludia Jaczynska<sup>a,b,c</sup>, Victoria Esser<sup>a,b,c</sup>, Junjie Xu<sup>a,b,c</sup>, Levent Sari<sup>a,d</sup>, Milo M. Lin<sup>a,d</sup>,

Christian Rosenmund<sup>e,f</sup> and Josep Rizo<sup>a,b,c,1</sup>

<sup>a</sup>Department of Biophysics, University of Texas Southwestern Medical Center, Dallas, Texas 75390, USA

<sup>b</sup>Department of Biochemistry, University of Texas Southwestern Medical Center, Dallas, Texas 75390, USA

<sup>c</sup>Department of Pharmacology, University of Texas Southwestern Medical Center, Dallas, Texas 75390, USA

<sup>d</sup>Green Center for Systems Biology, University of Texas Southwestern Medical Center, Dallas, Texas 75390, USA

<sup>e</sup>Charité – Universitätsmedizin Berlin, corporate member of Freie Universität Berlin and Humboldt-Universität zu Berlin, Institute of Neurophysiology, Berlin, Germany

<sup>f</sup>NeuroCure Cluster of Excellence, Berlin, Germany.

<sup>1</sup>To whom correspondence may be addressed. Email: [Jose.Rizo-Rey@UTSouthwestern.edu](mailto:Jose.Rizo-Rey@UTSouthwestern.edu)

#### This PDF file includes:

Supplementary Discussion  
Supplementary Methods  
Tables S1 to S3  
Figures S1 to S20  
SI References

## Supplementary Discussion

The model of Fig. 5A assumes that, in the primed state existing before  $\text{Ca}^{2+}$  influx, the Syt1 C<sub>2</sub>B domain binds to the SNARE complex through the primary interface and to the plasma membrane through the polybasic region, resulting in an approximately parallel orientation of the C<sub>2</sub>B domain with respect to the plasma membrane. The  $\text{Ca}^{2+}$ -activated state of Fig. 5B was built manually in Pymol assuming that  $\text{Ca}^{2+}$ -binding induces an approximately perpendicular orientation of the C<sub>2</sub>B domain with respect to the membrane, similar to that determined by electron paramagnetic resonance when C<sub>2</sub>B domain binds to SNARE-free membranes in the presence of  $\text{Ca}^{2+}$  (1), and that the reorientation pulls the SNARE complex through electrostatic interactions of the C<sub>2</sub>B domain arginines of region II with SNARE acidic residues. The changes in FRET observed for the 27-412 and 34-412 pairs, as well as the lack of FRET changes for the 34-391 pair (Fig. 6) show that  $\text{Ca}^{2+}$  indeed induces reorientation of the C<sub>2</sub>B domain with respect to liposome-anchored SNARE complex and agree qualitatively with the models of Fig. 5A,B. However, we did not attempt to do a quantitative comparison of the FRET changes with the distances between the probes predicted by the models (see legend of Fig. 6) because there is a large uncertainty in the configuration of the  $\text{Ca}^{2+}$ -activated state and relatively small changes in the predicted angle of rotation of the C<sub>2</sub>B domain induced by  $\text{Ca}^{2+}$  lead to considerably large changes in the expected distances between the probes for the 27-412 and 34-412 pairs (but much smaller changes for the 34-391 pair). Moreover, the rotation might be transient or considerably smaller than that depicted in Fig. 5A,B, as small structural changes may be sufficient to trigger neurotransmitter release based on the energy considerations discussed below. In addition, a subset of the C<sub>2</sub>AB-SNARE-complexes used for the FRET measurements are located inside the liposomes and hence are inaccessible to the added  $\text{Ca}^{2+}$ .

It is also worth noting that Syt1 C<sub>2</sub>AB binds with similar affinities to nanodiscs containing or lacking SNARE complex in the presence of  $\text{Ca}^{2+}$  (2), which suggested that C<sub>2</sub>AB does not interact with the membrane-anchored SNARE complex or that binding is rather weak. While our FRET data now show that

C<sub>2</sub>AB does remain bound to membrane-anchored SNARE complex upon Ca<sup>2+</sup> binding (Fig. 6D), a potential concern about our model is whether the underlying Syt1-SNARE interactions are too weak to trigger neurotransmitter release. In this context, it is important to consider that Ca<sup>2+</sup> increases the rate of release in hippocampal neurons by about 18,000/70,000-fold (3, 4), which translates to a decrease in the energy barrier for release of 9.8-11.2 k<sub>B</sub>T. If at least three Syt1-SNARE complexes trigger release (5), the contribution of each complex to lower the energy barrier might be 3.3-3.7 k<sub>B</sub>T or less, which corresponds to a very weak binding energy and can be readily provided by electrostatic interactions and hydrogen bonds of the C<sub>2</sub>B domain arginines with the SNARE acidic residues in region II of the primary interface.

### Supplementary Methods

**MD simulations.** All-atom MD simulations were performed using Gromacs (6, 7) with the CHARMM36 force field (8). Solvation and ion addition for system setup were performed at the BioHPC supercomputing facility of UT Southwestern. Minimizations, equilibration steps and production molecular dynamics (MD) simulations were carried out on Frontera at the Texas Advanced Computing Center (TACC). Pymol (Schrödinger, LLC) was used for system design, manual manipulation and system visualization.

The methodology used to set up the systems and run MD simulations was analogous to that described previously (9, 10). The lipid compositions of the vesicle and the flat bilayers resembled those of synaptic vesicles and plasma membranes, respectively (11, 12), and are listed in Table S1 together with other parameters of the simulations. All systems were solvated with explicit water molecules (TIP3P model), adding potassium and chloride ions to reach a concentration of 145 mM and make the system neutral. All Syt1 C<sub>2</sub>AB molecules had five Ca<sup>2+</sup> ions placed at the corresponding binding sites (13, 14) except for those of the s1action2 simulation, which was Ca<sup>2+</sup>-free. No restraints were used to keep the Ca<sup>2+</sup> ions bound and no dissociation was observed during the simulations.

For all systems, we used the same vesicle generated previously (24) and moved lipids manually to accommodate different positions of the SNARE TM regions. The cac2absc simulation used the same bilayer and SNARE complexes used for the prsg simulation of (10). The four C<sub>2</sub>AB molecules were placed manually at positions interspersed between the four SNARE complexes, with the Ca<sup>2+</sup>-binding loops pointing toward the flat bilayer but without being in contact with it (Fig. S1A). The fusion2g system was analogous to the cac2absc system but using four copies of the SNARE complex that was almost fully assembled in fusion2g and placing the C<sub>2</sub>AB molecules with the Ca<sup>2+</sup> binding loops pointing toward the center of the vesicle-flat bilayer interface (Fig. S2A). The nosytfusion system had the same initial configuration of the fusion2g system but without C<sub>2</sub>AB molecules (Fig. S3A). The sytfusion2g system also had a configuration analogous to fusion2g but with only two C<sub>2</sub>AB molecules that had the Ca<sup>2+</sup>-binding loops pointing in the same direction, toward the center of the vesicle-flat bilayer interface (Fig. S4A). The sytfusion3 system included a vesicle, a flat bilayer and four trans-SNARE complexes placed closer to the center of the bilayer-bilayer interface, compared to the systems of Fig. S1A-S4A, as in the fusion2g simulation of (9). A restrained MD simulation was used to pull the syntaxin-1 TM regions to designed positions such that the distance between the vesicle and the flat membrane was increased by 1.6 nm to allow sufficient space to place four C<sub>2</sub>AB molecules poised to bridge the two membranes (Fig. S5A). The s1action2 system was built with a vesicle and the same flat bilayer used for the prsg simulation of (10), which is larger than that of the other simulations described here to provide sufficient space for interaction with C<sub>2</sub>AB molecules. The four trans-SNARE complexes were almost fully assembled and were placed at a distance from the bilayer-bilayer interface that was intermediate between those used for the prsg simulation of (10) and for the fusion2g simulation of (9). Each SNARE complex had a C<sub>2</sub>AB bound through the primary interface (Fig. S18A).

Systems were energy minimized using double precision, whereas the default mixed precision was used in all MD simulations. The systems were heated to the desired temperature running a 1 ns simulation in the NVT ensemble with 1 fs steps, and then equilibrated to 1 atm for 1 ns in the NPT ensemble with

isotropic Parrinello-Rahman pressure coupling (15) and 2 fs steps. NPT production MD simulations were performed for the times indicated in Table S1 using 2 fs steps, isotropic Parrinello-Rahman pressure coupling and a 1.1 nm cutoff for non-bonding interactions. Three different groups of atoms were used for Nose-Hoover temperature coupling (16): i) protein atoms; ii) lipid atoms; and iii) water and KCL ions. Periodic boundary conditions were imposed with Particle Mesh Ewald (PME) (17) summation for long-range electrostatics.

### **Protein expression and purification**

The rat synaptobrevin-2 SNARE motif (residues 29–93), rat syntaxin-1A SNARE motif (residues 191–253), human fragments of SNAP-25A encoding its SNARE motifs (residues 11–82, referred to as SNAP-25\_N, and residues 141–203, referred to as SNAP25\_C; both SNAP-25 fragments including tryptophan at the N-terminus to facilitate detection by UV spectroscopy), rat complexin-1 fragment (residues 26–83), full-length rat complexin-1, and the MSP1E3D1 protein scaffold for nanodiscsc (18) were expressed and purified as described in (2). Full-length rat syntaxin-1A, full-length *Cricetulus griseus* NSF, and full-length *Bos taurus*  $\alpha$ SNAP were expressed and purified as described in (19). The sequence of Syt1 C<sub>2</sub>AB fused through a 37-residue linker to the C-terminal SNARE motif of SNAP-25A (residues 141–204) (C<sub>2</sub>AB-linker-SNAP25\_C), as described in (20), was subcloned from Addgene plasmid #70057 (p045) into the pGEX-KG vector. Synaptotagmin-1 C<sub>2</sub>B domain (residues 271–421) and C<sub>2</sub>AB fragment (residues 140–421) were expressed and purified as in (21, 22). As described in these studies, the following steps are necessary to achieve best purity of the Syt1 C<sub>2</sub>B domain and C<sub>2</sub>AB domain: treatment of the lysate with protamine sulfate, washes on the affinity column with CaCl<sub>2</sub>, and cation exchange chromatography in buffer containing CaCl<sub>2</sub>. Only the last peak of the cation exchange chromatogram contains the pure Syt1 fragments devoid of polyacidic contaminants. Following cation exchange, the last step of purification Syt1 C<sub>2</sub>B domain and C<sub>2</sub>AB fragment was size exclusion on Superdex 75 column (GE 16/60) in 20 mM HEPES pH

7.4 100 mM KCl 1 mM TCEP, unless specified otherwise. Syt1 C<sub>2</sub>AB-linker-SNAP25\_C was purified analogously to the C<sub>2</sub>AB fragment but, because the flexible linker is prone to degradation, the purification had to be performed quickly and at cold temperatures to minimize degradation.

Expression vectors for mutant proteins were generated using standard PCR-based techniques with custom designed primers. These mutants included: Syt1 C<sub>2</sub>B (residues 271–421) E295K/Y338A, Y338D/A402T, R322E/K325E/R281Q, R322E/K325E/E295A, R322E/K325E/Y338D, R322E/K325E/Y338W, R322E/K325E/A402T; Syt1 C<sub>2</sub>AB (residues 140–421) T285W; C<sub>2</sub>AB-linker-SNAP25\_C C277A/E412C, C277A/S391C; SNAP-25\_N (residues 11–82) E27C, Q34C and R59C. All mutant proteins were purified as the WT proteins, including 0.5 mM TCEP in the final purification step for cysteine containing proteins. Isotopically labeled and perdeuterated Syt1 C<sub>2</sub>B domains were expressed using M9 expression media in 99.9% D<sub>2</sub>O with D-glucose (1,2,3,4,5,6,6-D<sub>7</sub>, 97–98%) as the sole carbon source (3 g/L) and <sup>15</sup>NH<sub>4</sub>Cl as the sole nitrogen source (1 g/L). Specific <sup>13</sup>CH<sub>3</sub>-labeling of the Met and Ile δ1 methyl groups of Syt1 C<sub>2</sub>B domains was achieved by adding [3,3-<sup>2</sup>H] <sup>13</sup>C-methyl α-ketobutyric acid (80 mg/L) and <sup>13</sup>C-methyl methionine (250 mg/L) (Cambridge Isotope Laboratories) to the cell cultures 30 min prior to IPTG induction. Syt1 C<sub>2</sub>B R322E/K325E/R281A was the only mutant used for NMR spectroscopy that was expressed without perdeuteration and methyl labelling. All C<sub>2</sub>B, C<sub>2</sub>AB and C<sub>2</sub>AB-linker-SNAP25\_C fusion proteins were expressed overnight at 25 °C with 0.4 mM IPTG induction at OD 0.8.

### **NMR spectroscopy**

All NMR spectra were acquired at 25 °C on Agilent DD2 spectrometers equipped with cold probes operating at 600 or 800 MHz. Titrations of WT and mutant <sup>2</sup>H,<sup>15</sup>N-labeled Syt1 C<sub>2</sub>B domain specifically <sup>13</sup>CH<sub>3</sub>-labeled at the Ile δ1 and Met methyl groups (referred to as <sup>15</sup>N-C<sub>2</sub>B for simplicity) with SNARE complex four-helix bundle bound to a fragment spanning residues 26-83 of complexin-1 (referred to as

CpxSC) were performed as described in (2). Specific  $^{13}\text{CH}_3$  labeling was performed for acquisition of  $^1\text{H}$ - $^{13}\text{C}$  heteronuclear multiple quantum (HMQC) spectra with these samples, although no such spectra are described here. Because the R322E/K325E mutation increases the stability of the C<sub>2</sub>B domain and slows down H/D exchange (2, 21), some amide groups in the  $\beta$ -strands are not fully protonated after expression in D<sub>2</sub>O and purification in buffers containing H<sub>2</sub>O, resulting in signal loss for the corresponding peaks. All newly purified C<sub>2</sub>B mutants bearing the R322E/K325E mutation were incubated at RT for one week or at 37 °C for 15 hours to facilitate full exchange, but some amide groups were still not fully exchanged after this procedure. The titrations were performed in NMR buffer containing 20 mM HEPES (pH 7.4), 100 mM KCl, 1 mM EDTA, 1 mM TCEP, 10% D<sub>2</sub>O and protease inhibitor cocktail [which contained 1  $\mu\text{M}$  Antipain Dihydrochloride (Thermo Fischer Scientific: 50488492), 20  $\mu\text{M}$  Leupeptin (Gold Bio: L01025) and 0.8  $\mu\text{M}$  Aprotinin (Gold Bio: A655100)]. A  $^1\text{H}$ - $^{15}\text{N}$  TROSY-HSQC spectrum was acquired first for 32  $\mu\text{M}$  isolated  $^{15}\text{N}$ -C<sub>2</sub>B domain and additional  $^1\text{H}$ - $^{15}\text{N}$  TROSY-HSQC spectra were acquired after adding increasing concentrations of CpxSC to the sample, resulting in gradual dilution of the  $^{15}\text{N}$ -C<sub>2</sub>B domain. The protein concentrations of each titration step for each mutant are indicated in the legends of Fig. 4 and S15. Soluble SNARE complex was assembled as described in (2), concentrated at room temperature to a concentration above 250  $\mu\text{M}$  using a 30 kDa centrifugation filter (Amicon) and exchanged into NMR buffer using Zeba Spin Desalting Columns, 7K MWCO, 10 mL (Thermo Fisher). Complexin-1 (26–83) was also concentrated above 250  $\mu\text{M}$  using a 3 kDa centrifugation filter (Amicon) and exchanged into NMR buffer. SNARE-Complexin-1 (26–83) complex was preassembled with 20% excess Complexin-1 (26–83) before mixing with  $^{15}\text{N}$ -C<sub>2</sub>B domain. Total acquisition times ranged from 3.5 to 87.5 hr, depending on the sensitivity of the spectra. All NMR data were processed with NMRPipe (23) (Delaglio et al., 1995) and analyzed with NMRViewJ (24).

### **Labeling proteins with fluorescent tags**

SNAP-25\_N R59C mutant was labeled with Monobromobimane (mBBr), Thermo Fisher Scientific (M20381). mBBr delivered in powder was solubilized using DMSO to 10 mM stock concentration freshly before labeling reaction. After affinity tag cleavage, SNAP-25\_N R59C was treated with 10X molar excess DTT and subjected to size exclusion chromatography (SEC) on a Superdex 75 column (GE 16/60) in labeling buffer (20 mM HEPES pH 7.4 125 mM KCl). Labelling was performed in a solution of 72  $\mu$ M protein with 10X molar excess mBBr overnight at 4°C while rotating, and excess dye was removed by SEC.

SNAP-25\_N Q34C and E27C mutants and C2AB-linker-SNAP25\_C single cysteine mutants were labeled with the photostable Trolox-Cy3 and Trolox-Cy5 derivatives (25) conjugated with maleimide, respectively (LD550-MAL and LD650-MAL, Lumidyne Technologies). Lumidyne dyes delivered in powder were solubilized using DMSO to 10 mM stock concentration and stored in 10  $\mu$ L aliquots at -80°C after solubilization. After cation exchange purification, C2AB-linker-SNAP25\_C single cysteine mutants were quickly buffer exchanged to 20 mM HEPES pH 7.4 100 mM KCl 0.5 mM TCEP using a PD-10 column. For the SNAP-25\_N single cysteine mutants the last purification step after affinity tag cleavage was size exclusion chromatography on a Superdex 75 column (GE 16/60) with the labeling buffer 20 mM HEPES pH 7.4 100 mM KCl 0.5 mM TCEP. The buffer exchanged proteins at a concentration of 50–100  $\mu$ M were incubated with 3X molar excess dye overnight at 4°C. The dye was added gently, preferably while stirring to avoid high local concentrations of DMSO. The reaction was quenched by addition of 10 mM DTT. Unreacted dye was separated from labeled protein by passing through a PD-10 column followed by size exclusion chromatography on a Superdex 75 column (GE 16/60). The concentration and the labeling efficiency of the tagged proteins were determined using UV-vis spectroscopy.

### **Bimane fluorescence quenching assay**

All fluorescence emission scans were collected on a PTI Quantamaster 400 spectrofluorometer (T-format) at room temperature with slits set to 1.25 mm. For tryptophan-induced bimane fluorescence quenching



assays, we used SNARE complexes anchored on nanodiscs as described (2) and labeled with bimane at position R59C of SNAP-25\_N. The lipid composition of nanodiscs was 84% POPC, 15% DOPS, 1% PIP<sub>2</sub>. The experiments were performed in 25 mM HEPES pH 7.4 100 mM KCl 0.1 mM TCEP 2.5 mM MgCl<sub>2</sub>, 2 mM ATP 1 mM EGTA containing 1.5 μM BSA to prevent sample binding to the cuvette. Fluorescence emission spectra (excitation at 380 nm) were acquired for samples containing 1 μM SC-59-bimane-nanodiscs alone or in the presence of 4 μM C<sub>2</sub>A-T285W without or with 2.0 mM CaCl<sub>2</sub> (1.0 mM free Ca<sup>2+</sup>).

### **Preparation of C<sub>2</sub>AB-SNARE-Complex-liposomes**

To prepare liposomes containing C<sub>2</sub>AB covalently linked to the SNARE complex, we used a lipid mixture including 84% POPC, 15% DOPS, 1% PIP<sub>2</sub>. Lipids were blow-dried under a stream of nitrogen, tilting and rotating the tube to form a thin film on the wall of the tubes. If precipitation was observed in the lipid mixture due to PIP<sub>2</sub> addition, the tube was incubated in 45 °C until solution cleared before drying. The tube with lipid film was then incubated in the vacuum desiccator overnight for further drying. Detergent solubilized C<sub>2</sub>AB-SNARE complex was formed by incubating 0.25 μM Trolox-Cy3-labeled SNAP-25\_N E27C or Q34C with 0.3 μM full-length rat syntaxin-1A, 0.3 μM synaptobrevin-2 (29–93) and 0.3 μM Trolox-Cy5-labeled C<sub>2</sub>AB-linker-SNAP25\_C S391C or E412C in the presence of 1% β-OG, 0.5 M NaCl and protease inhibitor cocktail overnight at 4°C. Next day, 25mM HEPES pH 7.4 100mM KCl buffer containing 2% (wt/vol) β-OG was added to hydrate the lipid film. The tube was vortexed vigorously for complete suspension (~2 min). The lipids were incubated at room temperature for 15 min and afterward sonicated in a bath sonicator for 5 min twice. After confirming formation of SDS-resistant C2AB-SNARE-complex by the SDS-PAGE, the complex was mixed with solubilized lipids in protein to lipid (P:L) ratio 1:5000 in the presence of 1% β-OG and incubated for 25 min at RT. The sample was dialyzed using the Thermo Scientific™ Slide-A-Lyzer™ Dialysis Cassettes MWCO 10kDa against 25mM HEPES pH 7.4 100mM KCl buffer containing Amberlite XAD-2 detergent-absorbing beads. The dialysis was started in 0.5 L buffer with 1 g XAD-2 and

incubated while mixing with a magnetic stirrer for 1 h in 4°C, changed to 0.5 L fresh buffer with 1 g XAD-2 and incubated for 1 h, and then changed again to 1 L fresh buffer with 2 g XAD-2 and dialyzed over-night (~12 h). The proteoliposomes were always kept on ice and used for the fluorescence experiments. Size distribution analysis by dynamic light scattering showed the average liposome radii was typically ~60–95 nm.

### **FRET assays**

All fluorescence emission scans were collected on a PTI Quantamaster 400 spectrofluorometer (T-format) at room temperature with excitation at 550 nm and slits set to 1.25 mm. Each sample contained 0.125 μM C<sub>2</sub>AB-SNARE-complex-liposomes in 25 mM HEPES pH 7.4 100 mM KCl buffer, 1 mM EGTA, 2.5 mM MgCl<sub>2</sub>, 2 mM ATP, 1.5 μM BSA, and 0.15 μM full-length Complexin-1. Mg-ATP and complexin-1 were included to hinder non-specific interactions. To examine the reproducibility of Ca<sup>2+</sup>-induced changes in FRET, spectra were acquired for separate samples prepared under identical conditions before and after addition of 2.0 mM CaCl<sub>2</sub> (1.0 mM free Ca<sup>2+</sup>). Because the Syt1 C<sub>2</sub>AB fragment and SNARE complex were fused covalently via the 37 aa linker and the SNARE complex is resistant to SDS, control spectra to measure the maximum donor fluorescence observable without FRET were acquired after incubation for 5 minutes at 37 °C with 0.4 μM NSF and 2 μM αSNAP (to disassemble the SNARE complex) in 25 mM HEPES pH 7.4 100 mM KCl buffer containing 1 mM EGTA, 2.5 mM MgCl<sub>2</sub>, 2 mM ATP, 1.5 μM BSA and 1% BOG. The presence of detergent proved to be necessary to recover maximum signal because a subset of the C<sub>2</sub>AB-SNARE-complexes get reconstituted inside the liposomes and hence are inaccessible to the disassembly machinery.

Table S1. Parameters of the MD simulations<sup>a</sup>.

<i>Vesicle</i>	CHL1	POPC	SAGL	SAPE	SAPI2D	SDPE	SDPS	SOPS	total	
Outer leaflet	1258	296	0	534	0	282	210	199	2779	
%	45.3	10.6	0	19.2	0	10.1	7.6	7.2		
Inner leaflet	814	668	0	183	0	99	1	1	1766	
%	46.1	37.8	0	10.4	0	5.6	0.1	0.1		
<i>Flat bilayer 1</i>	CHL1	POPC	SAGL	SAPE	SAPI2D	SDPE	SDPS	SOPS	total	
Upper leaflet	830	151	18	132	93	262	182	181	1849	
%	44.9	8.2	1.0	7.1	5.0	14.2	9.8	9.8		
Lower leaflet	810	774	18	72	0	126	0	0	1800	
%	45.0	43.0	1.0	4.0	0	7.0	0	0		
<i>Flat bilayer 2</i>	CHL1	POPC	SAGL	SAPE	SAPI2D	SDPE	SDPS	SOPS	total	
Upper leaflet	748	130	17	115	82	231	165	161	1649	
%	45.3	7.9	1.0	7.0	5.0	14.0	10.0	9.8	100	
Lower leaflet	720	688	16	64	0	112	0	0	1600	
%	45.0	43.0	1.0	4.0	0	7.0	0	0	100	
<i>Flat bilayer 3</i>	CHL1	POPC	SAGL	SAPE	SAPI2D	SDPE	SDPS	SOPS	total	
Upper leaflet	1035	184	23	161	115	322	230	230	2300	
%	45	8	1	7	5	14	10	10		
Lower leaflet	1009	964	22	88	0	154	0	0	2237	
%	45.1	43.1	1.0	3.9	0.0	6.9	0.0	0.0		
system name	flat bilayer	number of atoms	initial cell dimensions	length and temperature						
cac2absc	1	4921862	36.9 x 36.4 x 36.7 nm <sup>3</sup>	668 ns 310 K						
fusiong	1	4922564	36.9 x 36.4 x 36.7 nm <sup>3</sup>	510 ns 310 K						
nosytfusion	1	4921880	36.9 x 36.4 x 36.7 nm <sup>3</sup>	510 ns 310 K						
sytfusion2g	1	4920453	36.9 x 36.4 x 36.7 nm <sup>3</sup>	570 ns 310 K						
sytfusion3	2	4586690	35.6 x 36.8 x 35.3 nm <sup>3</sup>	450 ns 310 K						
s1action2	3	6745506	42.5 x 37.5 x 42.5 nm <sup>3</sup>	596 ns 310 K						

<sup>a</sup>All systems included four trans-SNARE complexes, a 24 nm vesicle and the indicated flat bilayer. The cac2absc, fusiong, sytfusion3 and s1action2 had four C<sub>2</sub>AB molecules, sytfusion2g had two and nosytfusion had none. C<sub>2</sub>AB molecules had five bound Ca<sup>2+</sup> ions except for those in s1action2, which was Ca<sup>2+</sup> free.

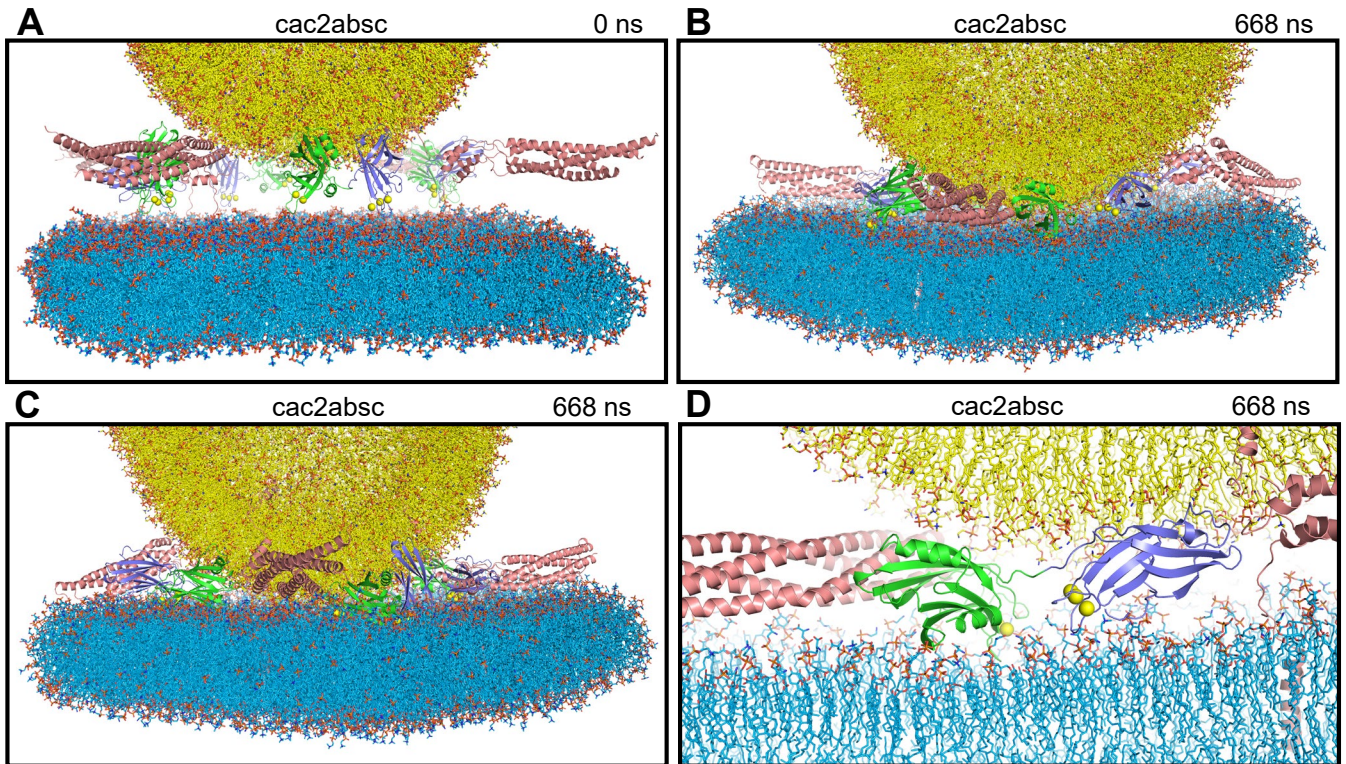
Table S2. Distances (Å) between the CZ atoms of arginines in region II of the primary interface and CG atoms of aspartes or CD atoms of glutamates of the SNAREs in crystal structures of Syt1-SNARE complexes<sup>a</sup>.

		5KJ7	5KJ8	5CCG	5CCH	5CCI	5W5C	5W5D
R281	D51	6.3	6.4	6.4	7.1	6.4	5.3	6
R282	E55	3.9	4	3.9	n.d.	4.1	4.5	4.5
R398	E55	10.8	11.7	10.7	n.d.	11.9	10.1	10.2
R398	D58	14.1	13.5	14.4	13.1	13.5	11.6	11.9
R398	E62	13.8	14.3	14.1	11.9	14.2	n.d.	n.d.
R398	E234	5	5.8	5.1	5.0	6.4	5.2	6.1
R398	E238	6.5	6.5	6.6	6.4	7.1	6.1	6.6
R399	E52	4.2	4.5	4.3	5.7	3.7	3.8	4.1
R399	D231	4.5	4.8	4.5	12.5	7.0	7.8	7.9
R399	E234	7.9	7.8	7.8	9.2	11.1	10.6	10.9

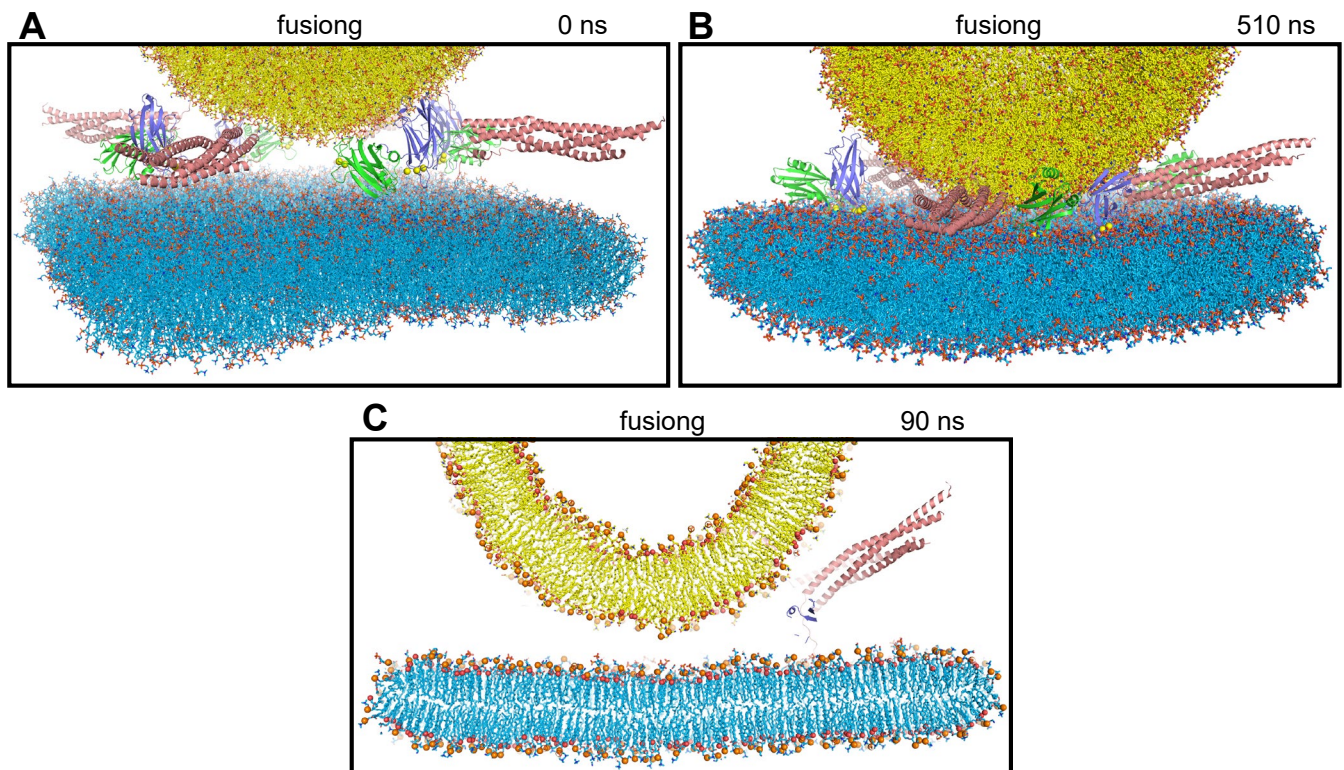
<sup>a</sup> n.d. = no density observed for that atom.

Table S3. Average distances (Å) between the CZ atoms of arginines in region II of the primary interface and CG atoms of aspartes or CD atoms of glutamates of the SNAREs in the four primed complexes (prcs) during the s1action2 MD simulation, and average distances for the four complexes of s1action 2 and the four complexes of the prsg MD simulation of ref. (10).

		prc-1	prc-2	prc-3	prc-4	S1action2 average	prsg average
R281	D51	4.1	4.0	4.1	3.9	4.0	4.0
R282	E55	4.5	4.6	4.3	4.5	4.5	4.5
R398	E55	6.8	6.7	7.9	6.8	7.0	5.7
R398	D58	7.6	7.6	10.0	7.2	8.1	6.0
R398	E62	5.7	4.4	8.3	4.9	5.8	5.9
R398	E234	8.3	9.4	7.2	9.1	8.5	10.9
R398	E238	9.0	10.4	7.3	10.4	9.3	17.0
R399	E52	5.7	8.4	5.2	5.6	6.2	5.5
R399	D231	7.0	9.1	7.3	7.2	7.6	6.6
R399	E234	6.3	6.3	8.7	7.1	7.1	8.1



**Figure S1.** MD simulation designed to investigate whether  $\text{Ca}^{2+}$ -saturated Syt1  $\text{C}_2$  domains spontaneously insert into the bilayers, perturb or bridge the bilayers (*cac2absc* simulation). (A) Initial configuration. (B, C) Configuration after 668 ns of simulation viewed from opposed angles. (D) Close-up view of the system at 668 ns showing a  $\text{C}_2\text{B}$  domain that is next to the C-terminus of a SNARE complex that is almost fully assembled and with the  $\text{Ca}^{2+}$ -binding loops oriented toward the center of the membrane-membrane interface. Lipids are represented by stick models, proteins by ribbon diagrams and  $\text{Ca}^{2+}$  ions by spheres with the same color coding as in Fig. 1.



**Figure S2.** MD simulation designed to examine whether the Ca<sup>2+</sup>-saturated Syt1 C<sub>2</sub> domains cooperate with almost fully assembled SNARE complexes to induce membrane fusion (fusing simulation). (A) Initial configuration. (B) Configuration after 510 ns of simulation. (C) Slice of the system after 90 ns of simulation showing how the membrane remained more distant than in an analogous simulation without Syt1 C<sub>2</sub>AB molecules (compared with Fig. S3C). Lipids are represented by stick models, proteins by ribbon diagrams and Ca<sup>2+</sup> ions by spheres with the same color coding as in Fig. 1.

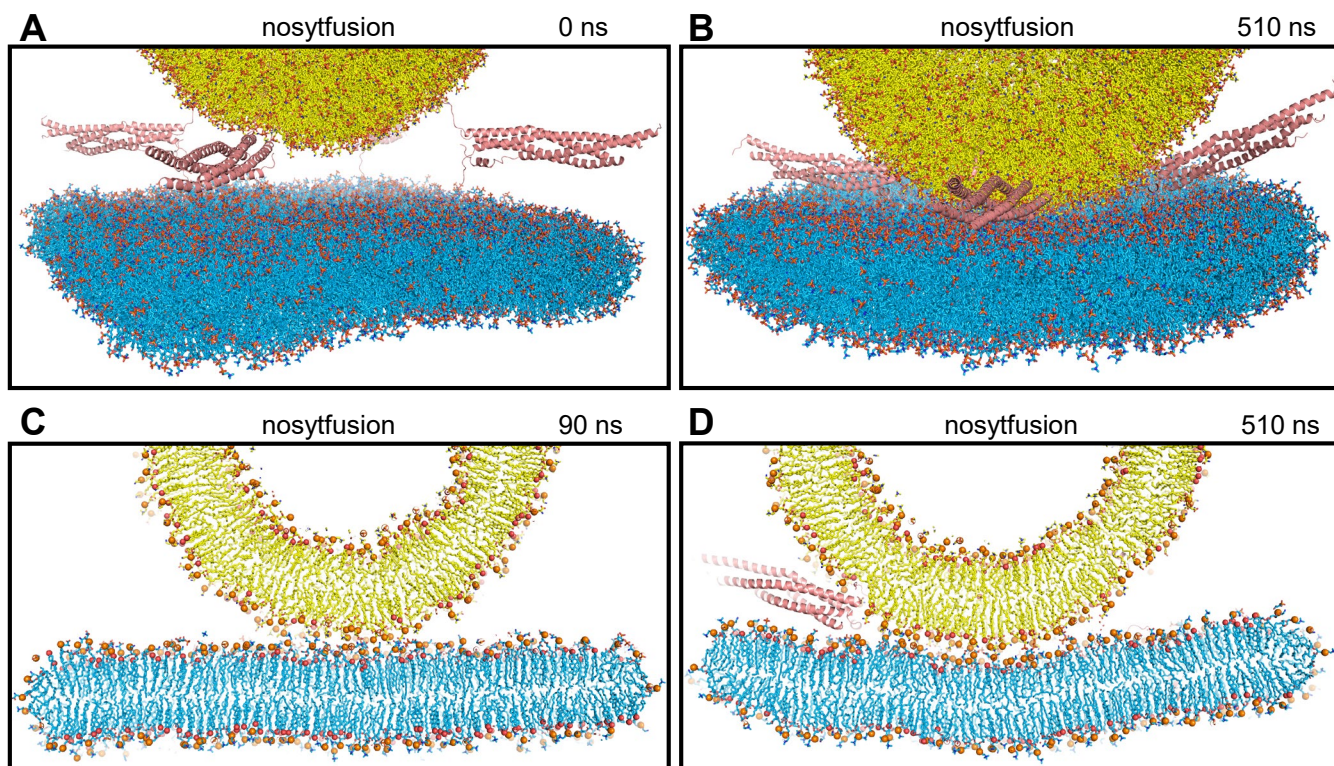


**Figure S3.** MD simulation of a system analogous to fusing but without  $C_2AB$  molecules to test whether they hinder the action of SNARE complexes in bringing membranes together (nosytfusion simulation). (A) Initial configuration. (B) Configuration after 510 ns of simulation. (C, D) Slices of the system after 90 ns (C) and 510 ns (D). Lipids are represented by stick models, proteins by ribbon diagrams and  $Ca^{2+}$  ions by spheres with the same color coding as in Fig. 1. Panel (C) shows how the membranes were already in contact at 90 ns, in contrast with the simulation that included  $C_2AB$  molecules (Fig. S2C). Panel (D) shows that the two membranes started to form an extended interface, unlike the simulation including  $C_2AB$  molecules (Fig. 1 b).

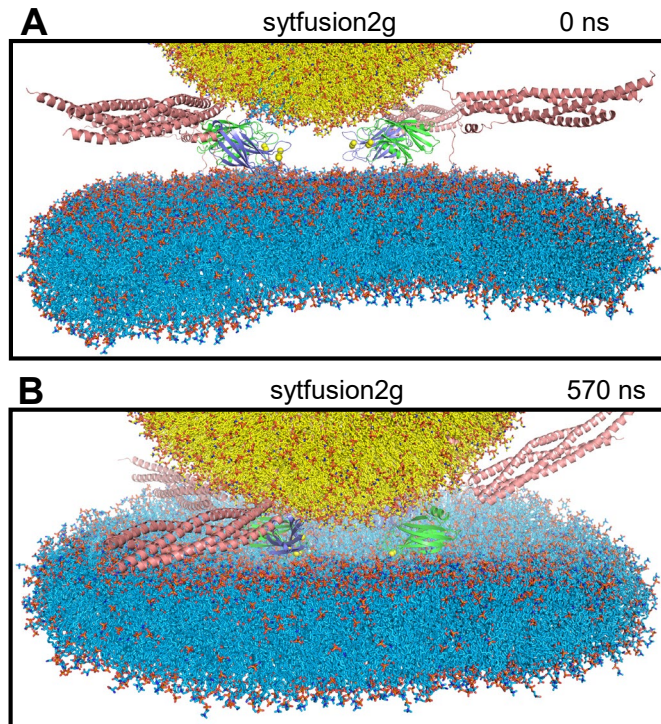


**Figure S4.** MD simulation with two  $\text{Ca}^{2+}$ -saturated Syt1  $\text{C}_2$  domains located between the two membranes to study whether they might play a direct role in membrane fusion (sytfusion2g simulation). Lipids are represented by stick models, proteins by ribbon diagrams and  $\text{Ca}^{2+}$  ions by spheres with the same color coding as in Fig. 1. (A) Initial configuration. (B) Configuration after 570 ns of simulation.



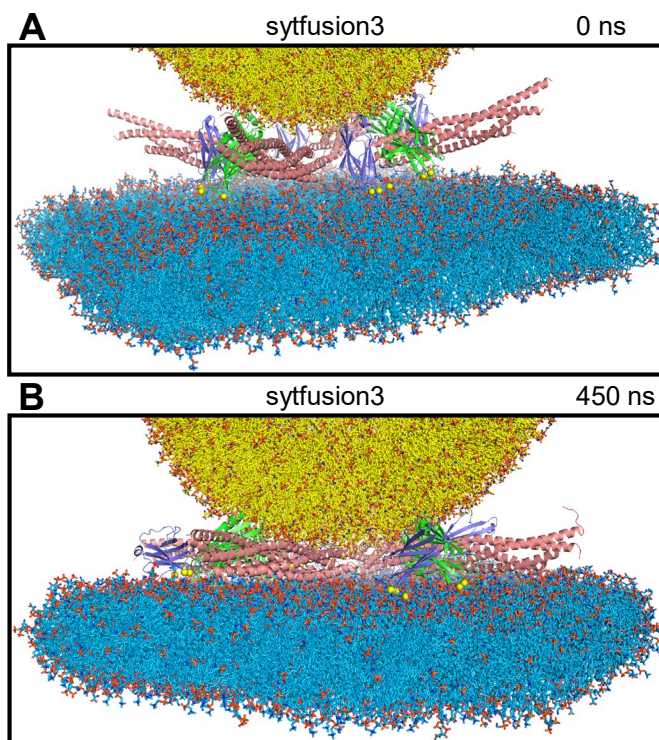


**Figure S5.** MD simulation designed to examine whether  $\text{Ca}^{2+}$ -saturated Syt1  $\text{C}_2$  domains might act as wedges that prevent the membranes from coming closer while the SNARE complexes pull the membranes together in the center to induce to torque forces that help to bend the membranes to initiate membrane fusion (sytfusion3 simulation). Lipids are represented by stick models, proteins by ribbon diagrams and  $\text{Ca}^{2+}$  ions by spheres with the same color coding as in Fig. 1. (A) Initial configuration. (B) Configuration after 450 ns of simulation.

## WT

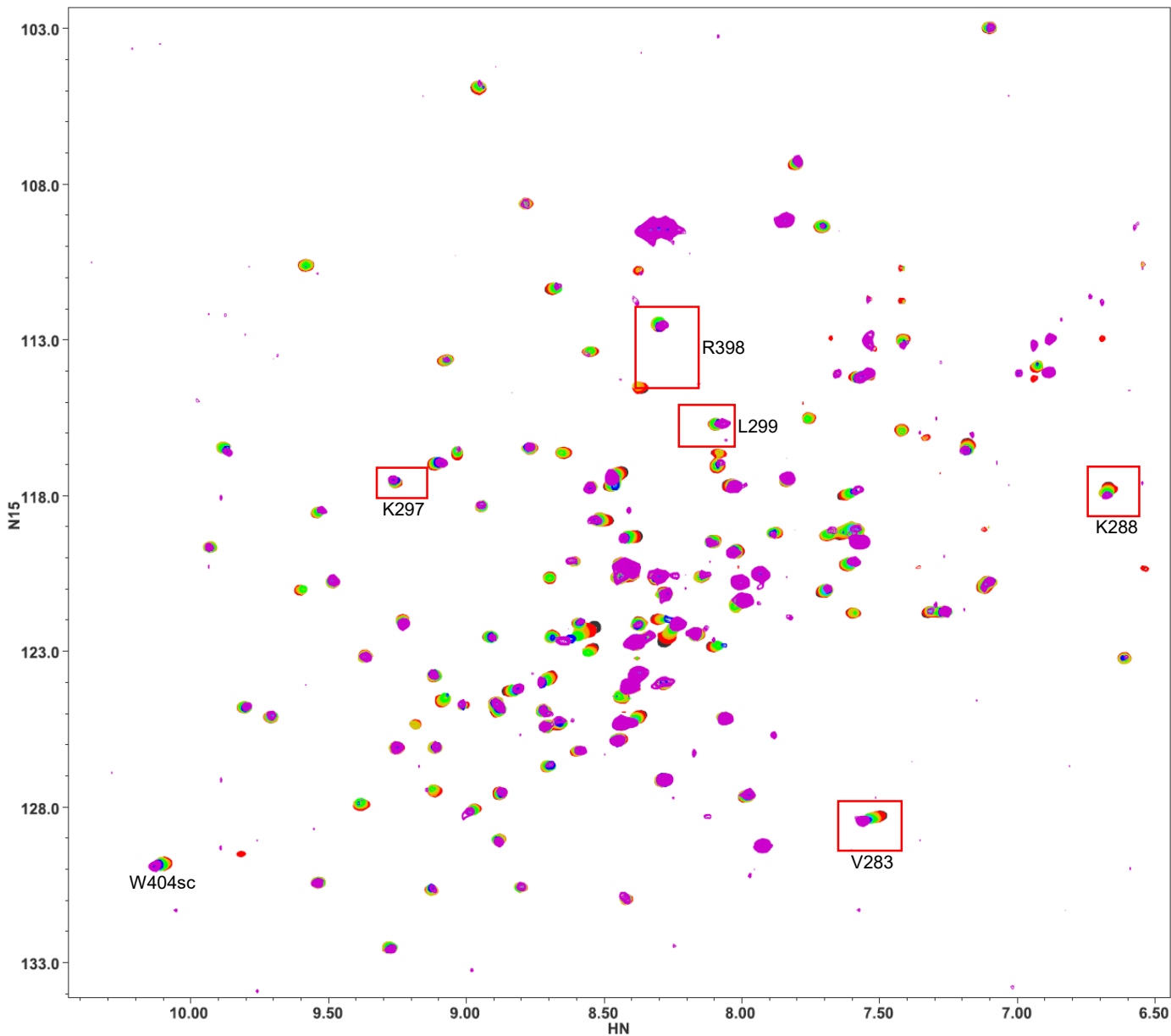


**Figure S6.** Superposition of  $^1\text{H}$ - $^{15}\text{N}$  TROSY-HSQC spectra of WT  $^{15}\text{N}$ -C<sub>2</sub>B domain in the absence of  $\text{Ca}^{2+}$  and the presence of increasing concentrations of CpxSC. The following concentrations of  $^{15}\text{N}$ -C<sub>2</sub>B and CpxSC ( $\mu\text{M}/\mu\text{M}$ ) were used (from black to purple): 32/0, 30/10, 28/19, 26/28, 24/36, 20/51, 17/64, 12/85. The intensities of cross-peaks decreased as CpxSC was added because  $^{15}\text{N}$ -C<sub>2</sub>B was diluted and binding to CpxSC causes cross-peak broadening. Contour levels were adjusted to compensate for these decreased intensities, but some cross-peaks may not be visible even after these adjustments at the higher CpxSC concentrations. The red boxes indicate the cross-peaks that are displayed in the expansions of Fig. S15B.

## E295K,Y338A

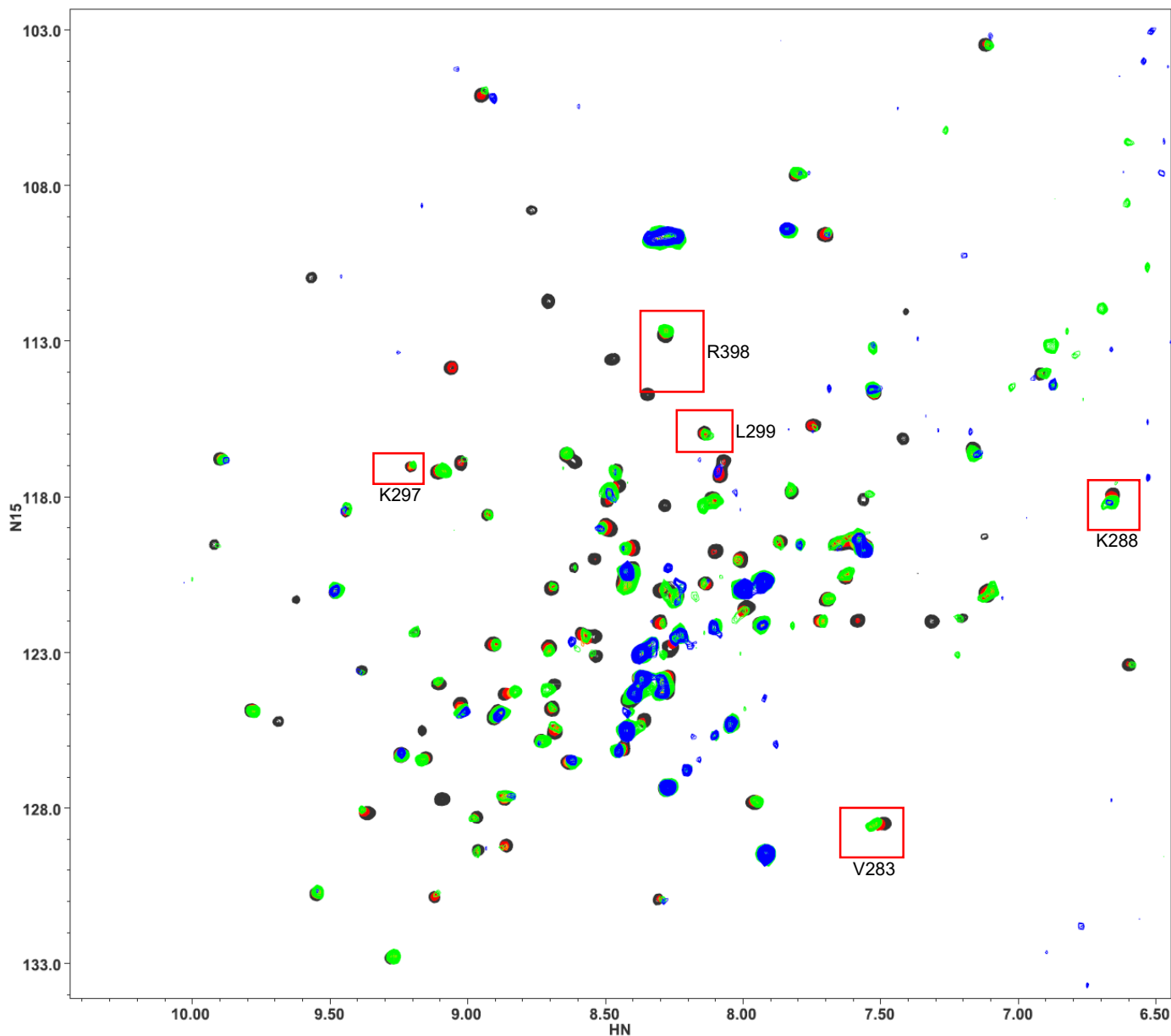


**Figure S7.** Superposition of  $^1\text{H}$ - $^{15}\text{N}$  TROSY-HSQC spectra of  $^{15}\text{N}$ -C<sub>2</sub>B domain E295K/Y338A mutant in the absence of  $\text{Ca}^{2+}$  and the presence of increasing concentrations of CpxSC. The following concentrations of  $^{15}\text{N}$ -C<sub>2</sub>B and CpxSC ( $\mu\text{M}/\mu\text{M}$ ) were used (from black to blue): 32/0, 30/11, 27/21, 25/30, 23/38, 19/59. The intensities of cross-peaks decreased as CpxSC was added because  $^{15}\text{N}$ -C<sub>2</sub>B was diluted and binding to CpxSC causes cross-peak broadening. Contour levels were adjusted to compensate for these decreased intensities, but some cross-peaks may not be visible even after these adjustments at the higher CpxSc concentrations. The red boxes indicate the cross-peaks that are displayed in the expansions of Fig. S15B.

### Y338D,A402T

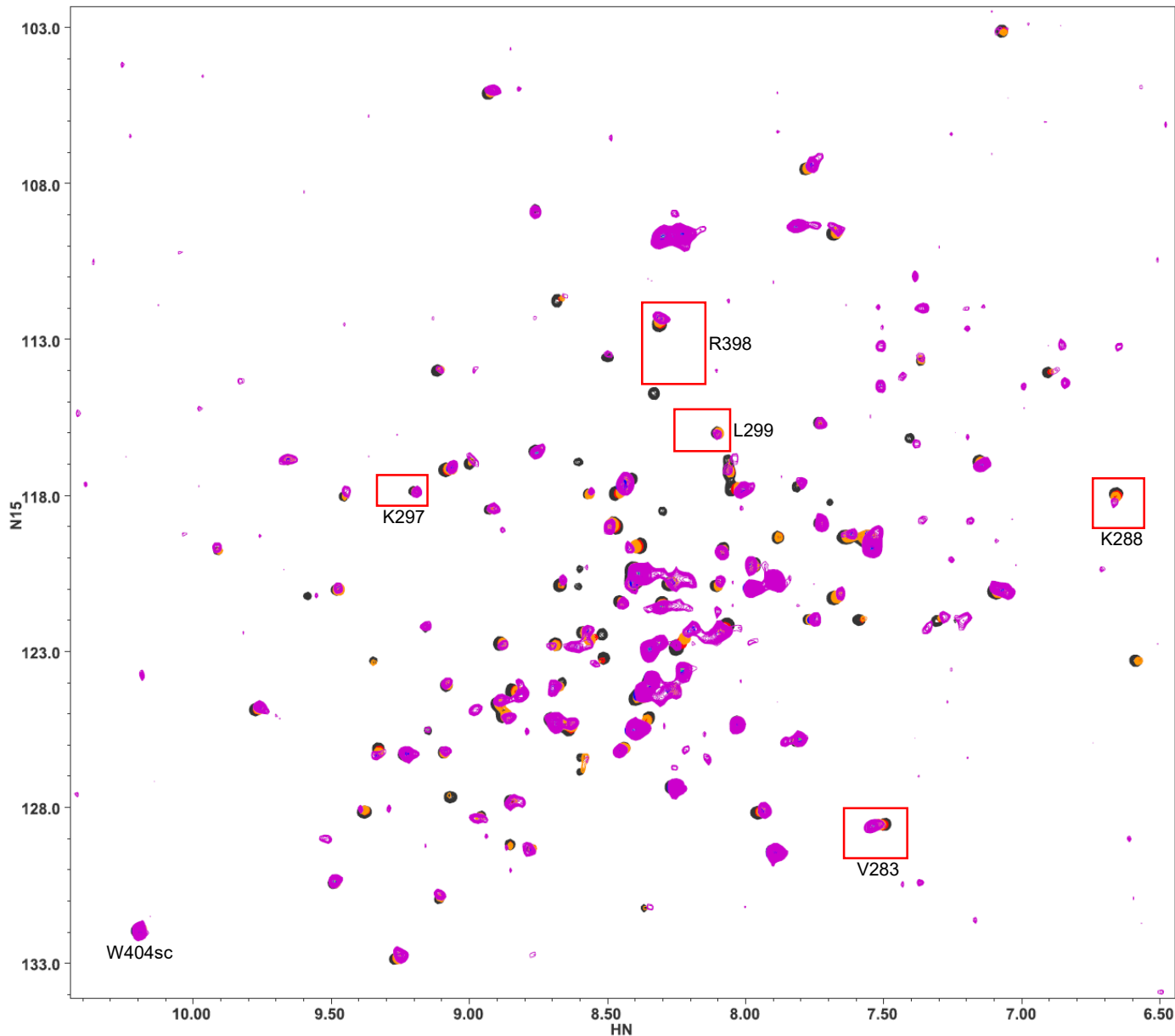


**Figure S8.** Superposition of  $^1\text{H}$ - $^{15}\text{N}$  TROSY-HSQC spectra of  $^{15}\text{N}$ -C<sub>2</sub>B domain Y338D/A402T mutant in the absence of  $\text{Ca}^{2+}$  and the presence of increasing concentrations of CpxSC. The following concentrations of  $^{15}\text{N}$ -C<sub>2</sub>B and CpxSC ( $\mu\text{M}/\mu\text{M}$ ) were used (from black to purple): 32/0, 30/10, 28/19, 26/28, 24/36, 20/51, 17/64, 12/86. The intensities of cross-peaks decreased as CpxSC was added because  $^{15}\text{N}$ -C<sub>2</sub>B was diluted and binding to CpxSC causes cross-peak broadening. Contour levels were adjusted to compensate for these decreased intensities, but some cross-peaks may not be visible even after these adjustments at the higher CpxSc concentrations. The red boxes indicate the cross-peaks that are displayed in the expansions of Fig. S15B.

## REKE

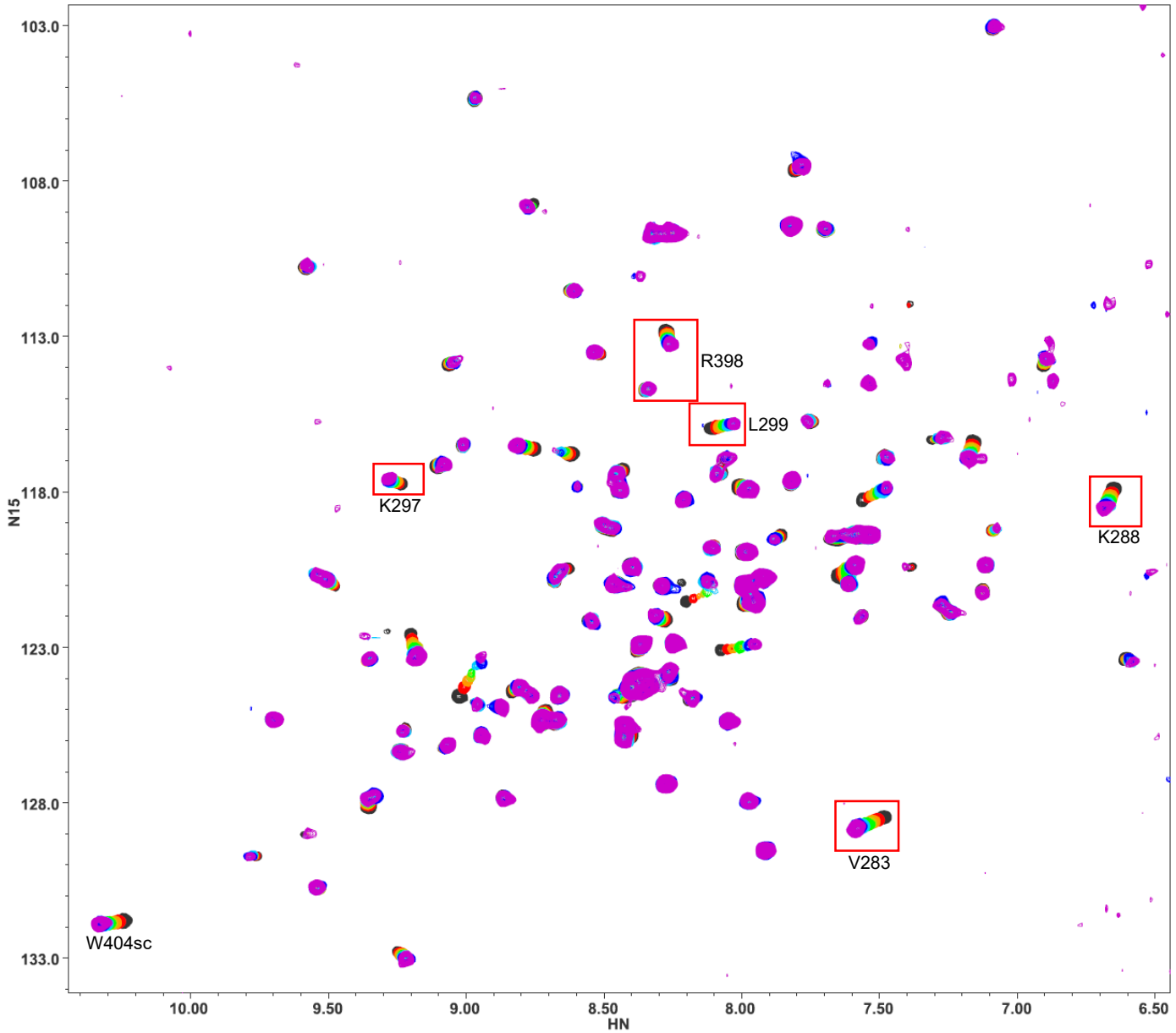


**Figure S9.** Superposition of  $^1\text{H}$ - $^{15}\text{N}$  TROSY-HSQC spectra of  $^{15}\text{N}$ -C<sub>2</sub>B domain REKE mutant in the absence of Ca<sup>2+</sup> and the presence of increasing concentrations of CpxSC. The following concentrations of  $^{15}\text{N}$ -C<sub>2</sub>B and CpxSC ( $\mu\text{M}/\mu\text{M}$ ) were used (from black to purple): 32/0, 30/10, 28/19, 26/28, 24/36, 20/51, 17/64, 12/85. The intensities of cross-peaks decreased as CpxSC was added because  $^{15}\text{N}$ -C<sub>2</sub>B was diluted and binding to CpxSC causes cross-peak broadening. Contour levels were adjusted to compensate for these decreased intensities, but some cross-peaks may not be visible even after these adjustments at the higher CpxSc concentrations. The red boxes indicate the cross-peaks that are displayed in the expansions of Fig. 4.

## REKE-R281A

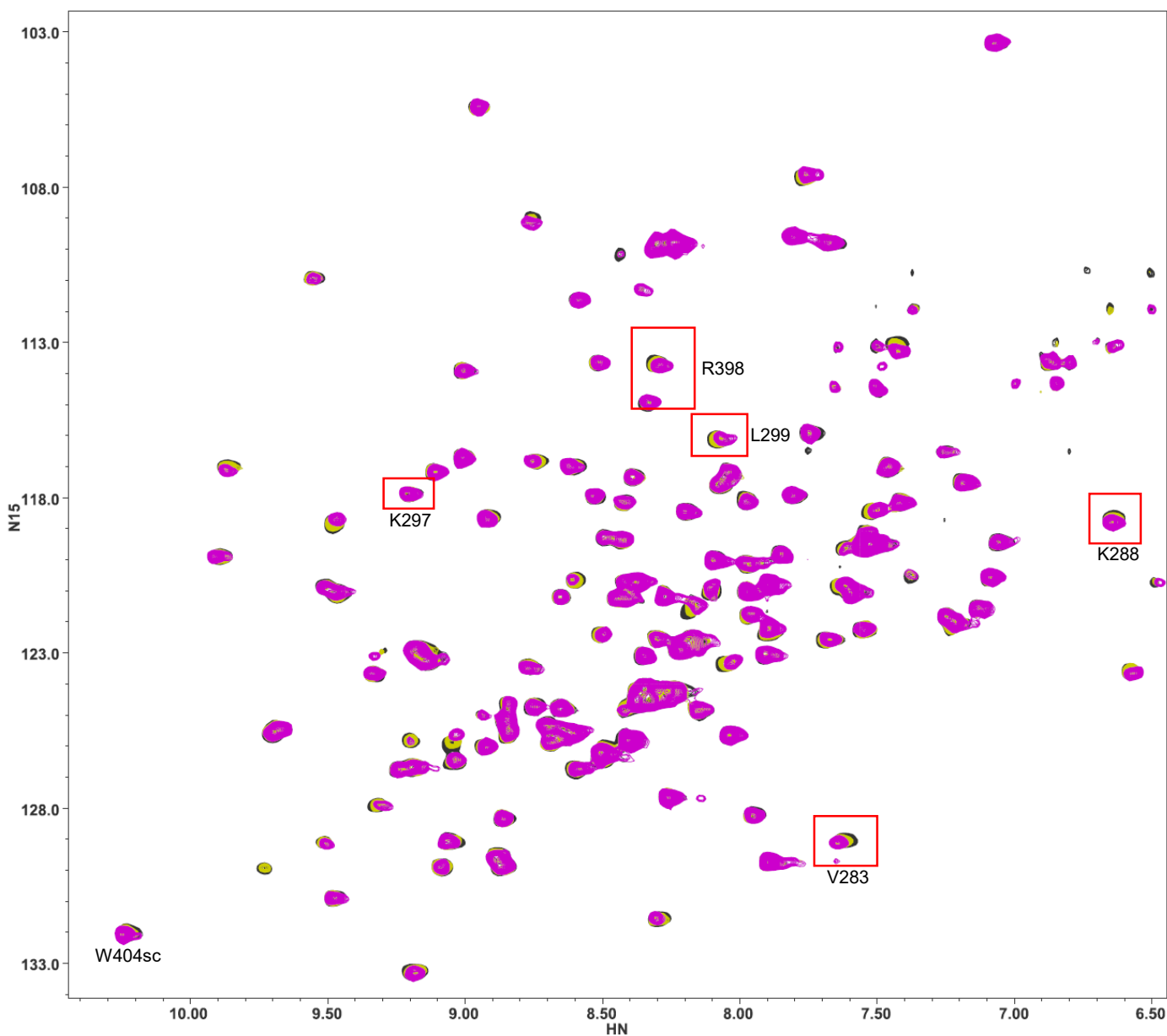


**Figure S10.** Superposition of  $^1\text{H}$ - $^{15}\text{N}$  TROSY-HSQC spectra of  $^{15}\text{N}$ -C<sub>2</sub>B domain REKE-R281A mutant in the absence of  $\text{Ca}^{2+}$  and the presence of increasing concentrations of CpxSC. The following concentrations of  $^{15}\text{N}$ -C<sub>2</sub>B and CpxSC ( $\mu\text{M}/\mu\text{M}$ ) were used: 32/0 (black), 26/28 (yellow) and 13/98 (purple). The intensities of cross-peaks decreased as CpxSC was added because  $^{15}\text{N}$ -C<sub>2</sub>B was diluted and binding to CpxSC causes cross-peak broadening. Contour levels were adjusted to compensate for these decreased intensities, but some cross-peaks may not be visible even after these adjustments at the higher CpxSC concentrations. The red boxes indicate the cross-peaks that are displayed in the expansions of Fig. 4.

## REKE-Y338W

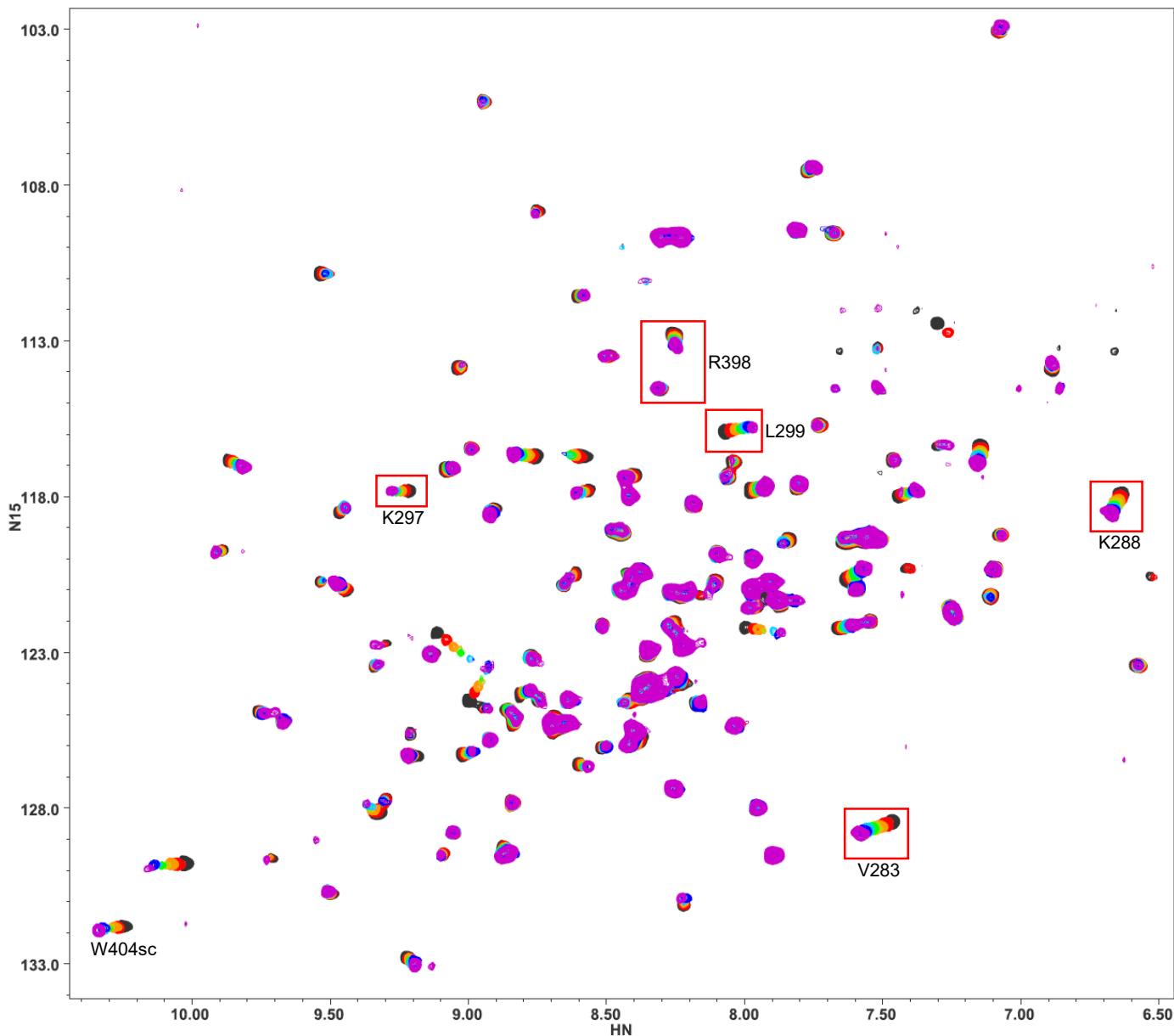


**Figure S11.** Superposition of  $^1\text{H}$ - $^{15}\text{N}$  TROSY-HSQC spectra of  $^{15}\text{N}$ -C<sub>2</sub>B domain REKE-Y338W mutant in the absence of Ca<sup>2+</sup> and the presence of increasing concentrations of CpxSC. The following concentrations of  $^{15}\text{N}$ -C<sub>2</sub>B and CpxSC ( $\mu\text{M}/\mu\text{M}$ ) were used (from black to purple): 32/0, 30/10, 28/19, 26/28, 24/36, 20/53, 17/67, 12/88. The intensities of cross-peaks decreased as CpxSC was added because  $^{15}\text{N}$ -C<sub>2</sub>B was diluted and binding to CpxSC causes cross-peak broadening. Contour levels were adjusted to compensate for these decreased intensities, but some cross-peaks may not be visible even after these adjustments at the higher CpxSc concentrations. The red boxes indicate the cross-peaks that are displayed in the expansions of Fig. 4.

## REKE-E295A

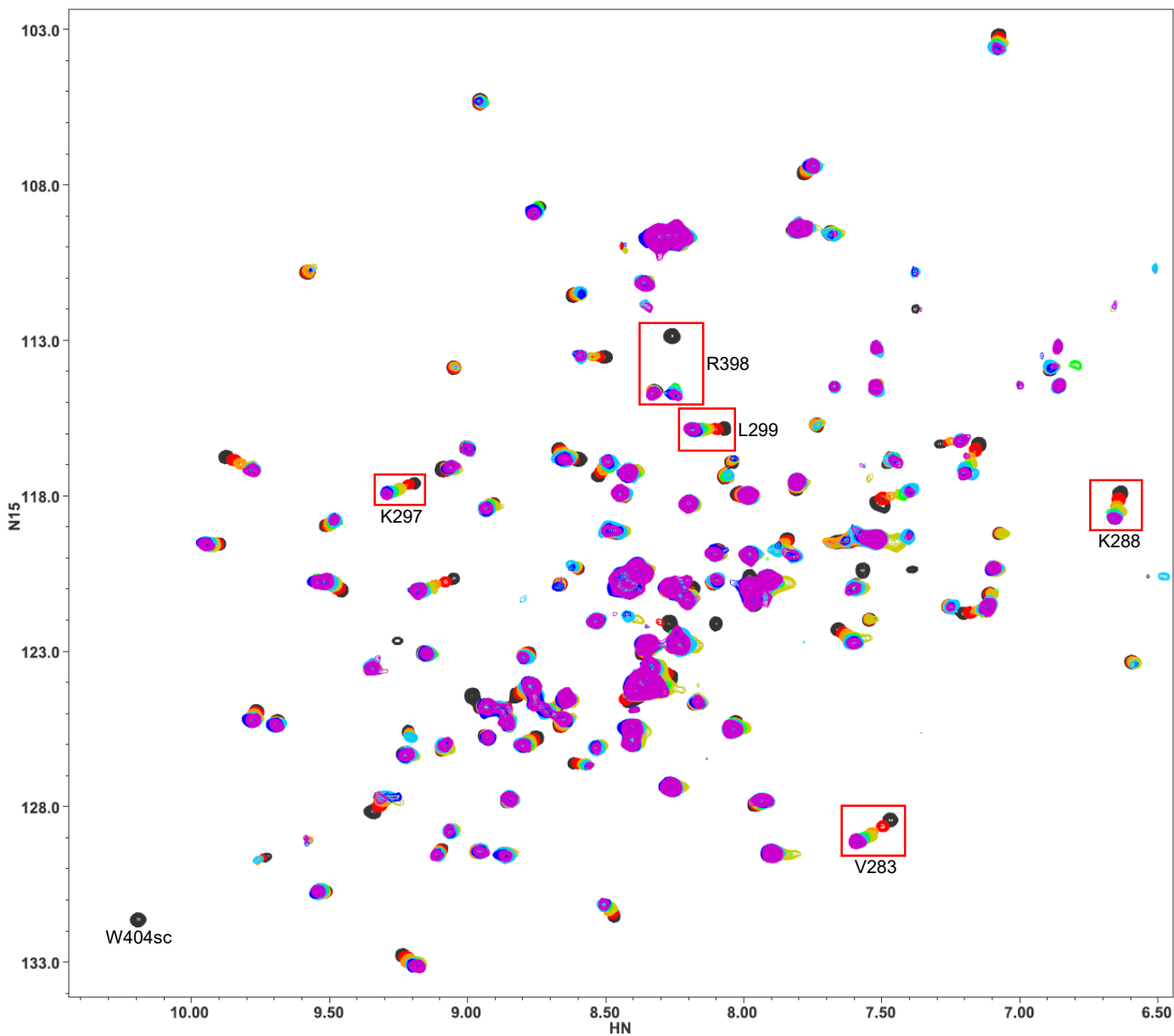


**Figure S12.** Superposition of  $^1\text{H}$ - $^{15}\text{N}$  TROSY-HSQC spectra of  $^{15}\text{N}$ -C<sub>2</sub>B domain REKE-E295A mutant in the absence of  $\text{Ca}^{2+}$  and the presence of increasing concentrations of CpxSC. The following concentrations of  $^{15}\text{N}$ -C<sub>2</sub>B and CpxSC ( $\mu\text{M}/\mu\text{M}$ ) were used (from black to purple): 32/0, 30/10, 28/19, 26/28, 24/36, 20/53, 17/65, 12/88. The intensities of cross-peaks decreased as CpxSC was added because  $^{15}\text{N}$ -C<sub>2</sub>B was diluted and binding to CpxSC causes cross-peak broadening. Contour levels were adjusted to compensate for these decreased intensities, but some cross-peaks may not be visible even after these adjustments at the higher CpxSc concentrations. In addition some of the cross-peaks in the middle of the titration are not observed because of chemical exchange broadening. The red boxes indicate the cross-peaks that are displayed in the expansions of Fig. 4.



## REKE-A402T

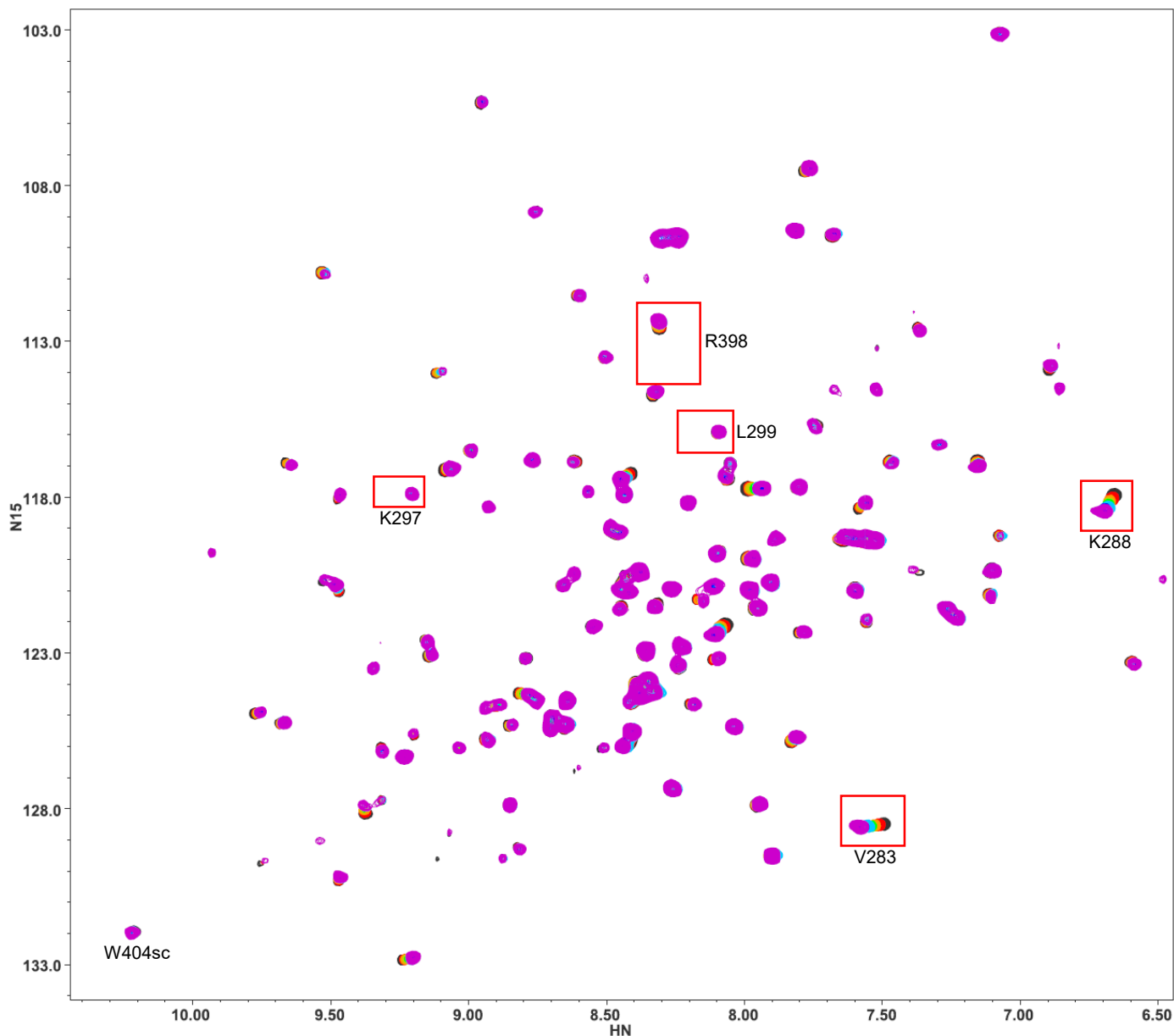


**Figure S13.** Superposition of  $^1\text{H}$ - $^{15}\text{N}$  TROSY-HSQC spectra of  $^{15}\text{N}$ - $\text{C}_2\text{B}$  domain REKE-A402T mutant in the absence of  $\text{Ca}^{2+}$  and the presence of increasing concentrations of CpxSC. The following concentrations of  $^{15}\text{N}$ - $\text{C}_2\text{B}$  and CpxSC ( $\mu\text{M}/\mu\text{M}$ ) were used (from black to purple): 32/0, 30/10, 28/19, 26/28, 24/36, 20/53, 17/67, 12/88. The intensities of cross-peaks decreased as CpxSC was added because  $^{15}\text{N}$ - $\text{C}_2\text{B}$  was diluted and binding to CpxSC causes cross-peak broadening. Contour levels were adjusted to compensate for these decreased intensities, but some cross-peaks may not be visible even after these adjustments at the higher CpxSC concentrations. The red boxes indicate the cross-peaks that are displayed in the expansions of Fig. 4.

## REKE-Y338D

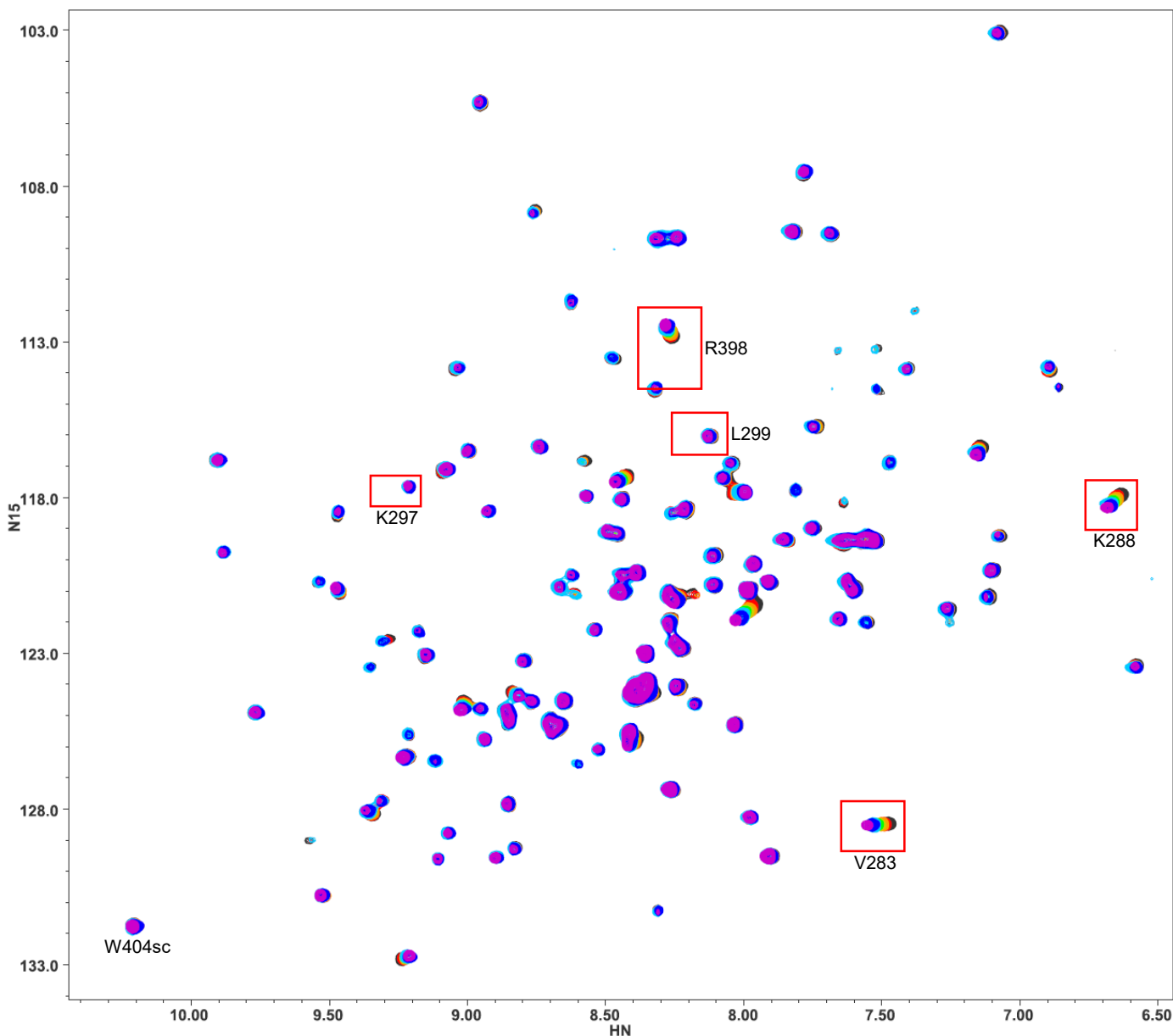


**Figure S14.** Superposition of  $^1\text{H}$ - $^{15}\text{N}$  TROSY-HSQC spectra of  $^{15}\text{N}$ -C<sub>2</sub>B domain REKE-Y338D mutant in the absence of  $\text{Ca}^{2+}$  and the presence of increasing concentrations of CpxSC. The following concentrations of  $^{15}\text{N}$ -C<sub>2</sub>B and CpxSC ( $\mu\text{M}/\mu\text{M}$ ) were used (from black to purple): 32/0, 30/10, 28/19, 26/28, 24/36, 20/53, 17/68, 12/88. The intensities of cross-peaks decreased as CpxSC was added because  $^{15}\text{N}$ -C<sub>2</sub>B was diluted and binding to CpxSC causes cross-peak broadening. Contour levels were adjusted to compensate for these decreased intensities, but some cross-peaks may not be visible even after these adjustments at the higher CpxSc concentrations. The red boxes indicate the cross-peaks that are displayed in the expansions of Fig. 4.

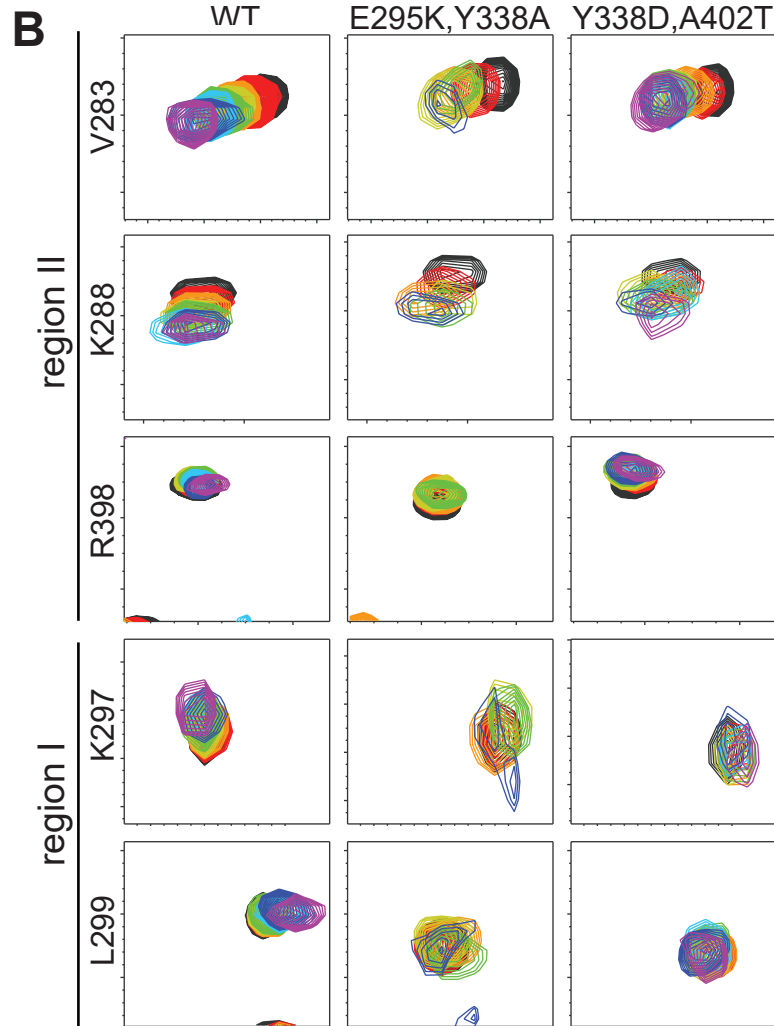
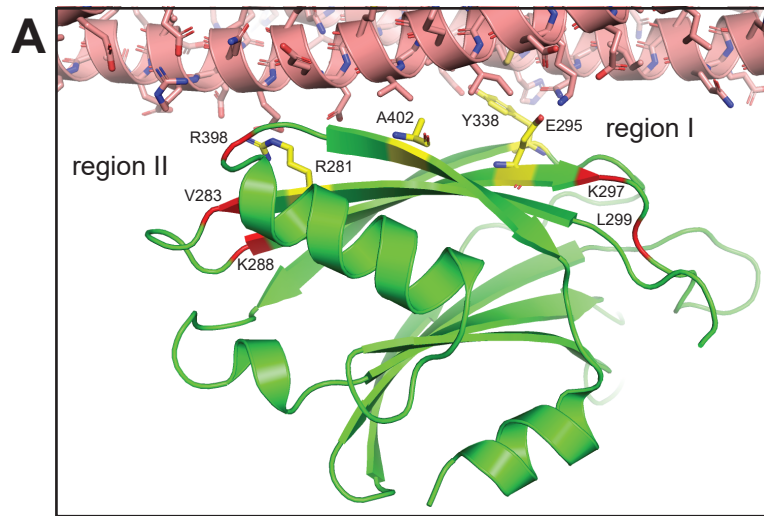


**Figure S15.** The Syt1 C<sub>2</sub>B domain still binds to the SNARE complex through region II of the primary interface when binding through region I is abolished. (A) Close-up view of the primary interface with the SNARE complex represented by a ribbon diagram and stick models (nitrogen atoms in dark blue, oxygen in red, sulfur in yellow orange and carbon in salmon color), and the Syt1 C<sub>2</sub>B domain represented by a green ribbon diagram and stick models for residues that were mutated in the NMR experiments of Fig. 4 and S6-S14 (carbon atoms in yellow). Residues corresponding to the cross-peaks shown in panel (B) and Fig. 4 are indicated in red on the ribbon diagram. These residues and those that were mutated are labeled. The diagram was generated with a crystal structure of a Syt1-SNARE complex (PDB accession number 5KJ7). (B) The diagrams show expansions of <sup>1</sup>H-<sup>15</sup>N TROSY HSQC spectra of WT and mutant <sup>15</sup>N-C<sub>2</sub>B domain (as indicated above) acquired in isolation (black contours) or increasing concentrations of CpxSC (rainbow colours). The residues corresponding to the cross-peaks shown in the expansions and the regions where they are located are indicated on the left. The following concentrations of <sup>15</sup>N-C<sub>2</sub>B mutant and CpxSC (μM/μM) were used (from black to purple): WT 32/0, 30/10, 28/19, 26/28, 24/36, 20/51, 17/64, 12/85; E295K/Y338A 32/0, 30/11, 27/21, 25/30, 23/38, 19/59; Y338D/A402T 32/0, 30/10, 28/19, 26/28, 24/36, 20/51, 17/64, 12/86. The intensities of cross-peaks decreased as CpxSC was added because <sup>15</sup>N-C<sub>2</sub>B was diluted and binding to CpxSC causes cross-peak broadening. Contour levels were adjusted to compensate for these decreased intensities.

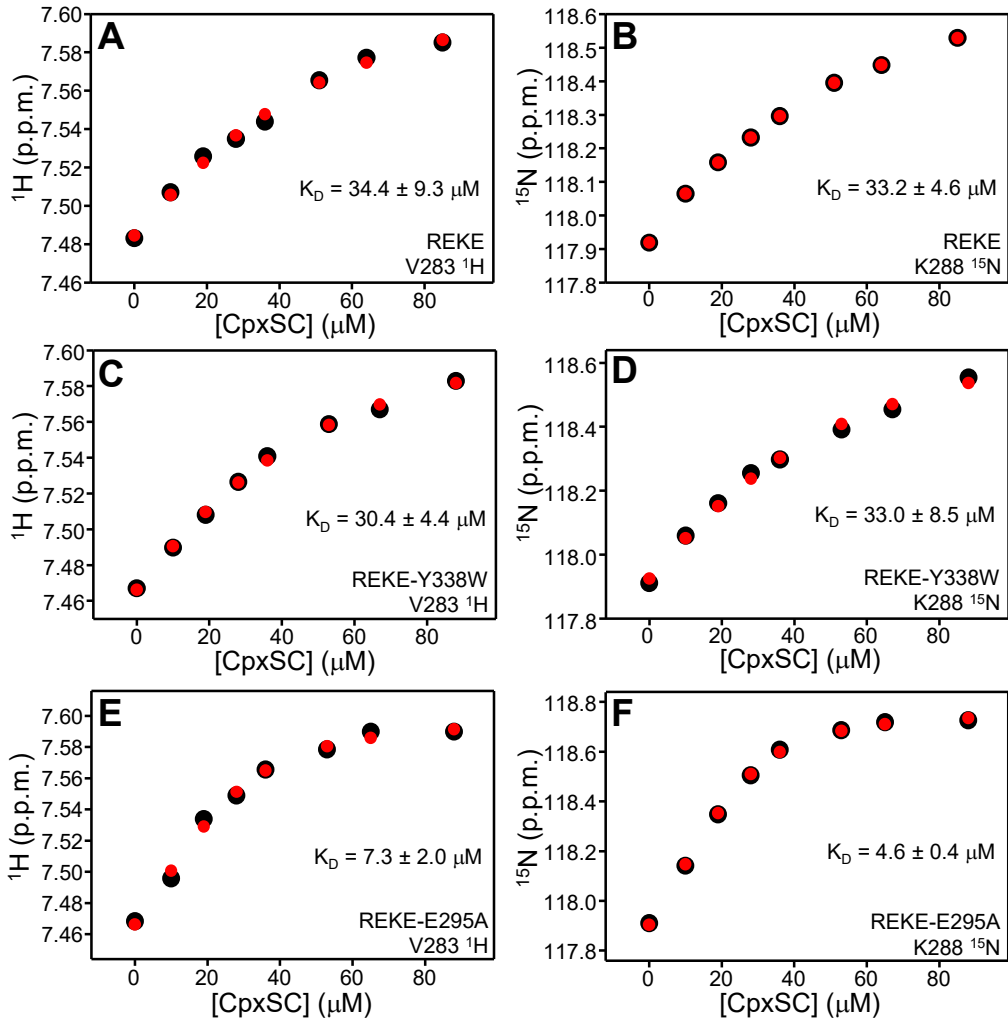


**Figure S16.** The E295A mutation enhances the affinity of the Syt1 C<sub>2</sub>B domain for the SNARE complex. (A-F) Plots of the <sup>1</sup>H chemical shift of the V283 cross-peak (A, C, E) or the <sup>15</sup>N chemical shift of the K288 cross-peak from REKE (A, B), REKE-Y338W (C, D) or REKE-E295A mutant <sup>15</sup>N-C<sub>2</sub>B domain in the titrations with CpxSC monitored by <sup>1</sup>H-<sup>15</sup>N TROSY-HSQC spectra (Fig. 4, S9, S11, S12). Note that the C<sub>2</sub>B domain concentration also changed during the titration as indicated in the corresponding figure legends. The black circles show the experimental data and the red circles show the predicted values after fitting the data to a single-site binding model using the equation  $f = d_0 + (d_f - d_0) \cdot (p + x + k - \sqrt{(p + x + k)^2 - 4 \cdot p \cdot x}) / (2 \cdot p)$ , where  $f$  is the corresponding chemical shift,  $d_0$  is the chemical shift of free <sup>15</sup>N-C<sub>2</sub>B domain,  $d_f$  is the chemical shift of CpxSC-saturated <sup>15</sup>N-C<sub>2</sub>B domain,  $p$  is the <sup>15</sup>N-C<sub>2</sub>B domain concentration,  $x$  is the CpxSC concentration and  $k$  is the K<sub>D</sub> (all concentrations in μM units). The K<sub>D</sub> values obtained for each graph are indicated together with the errors yielded by the fitting procedure.

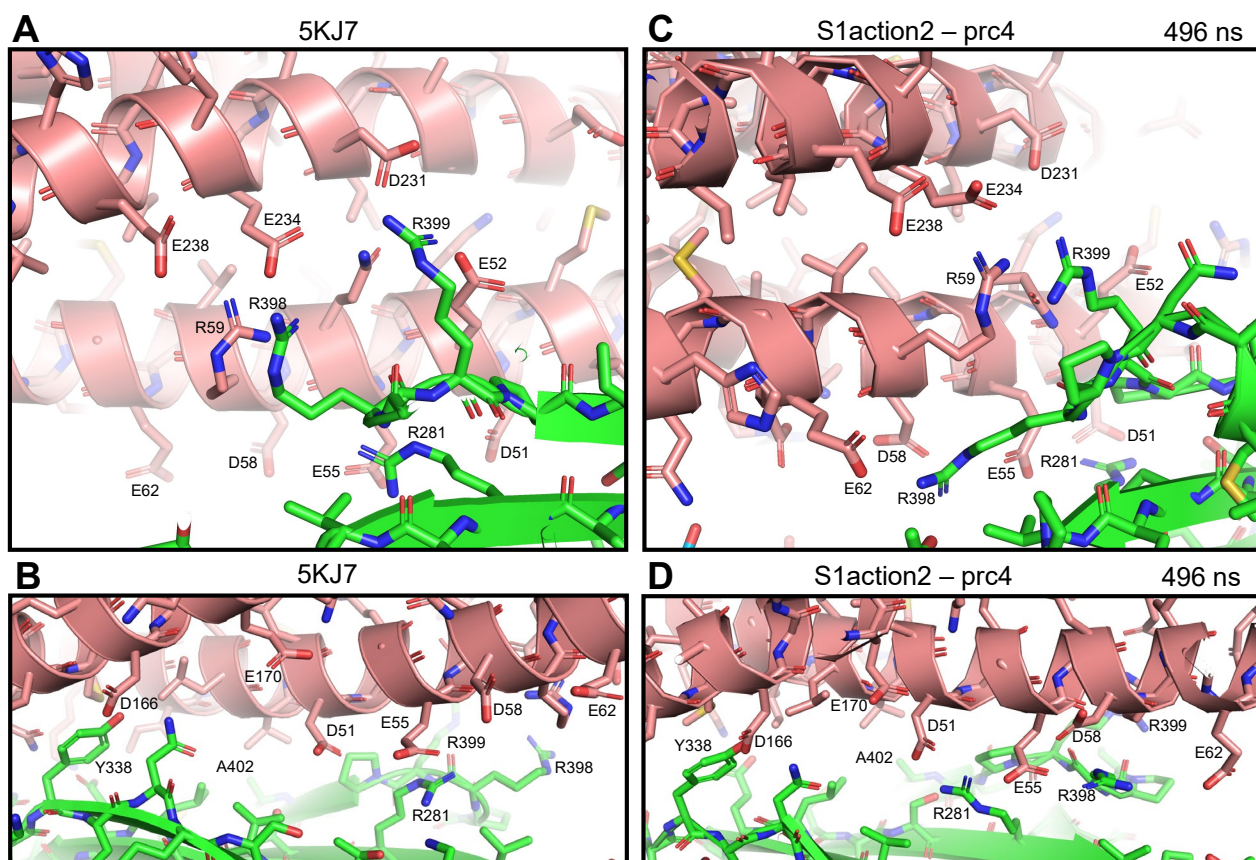


**Figure S17.** Diagrams illustrating differences observed in the primary interface of crystal structures of Syt1-SNARE complexes and in MD simulations. (A, B) Different views of region II a crystal structure of a Syt1-SNARE complex (PDB accession number 5KJ7). (C, D) Different views of region II of one of the primed complexes (prc4) at 496 ns of the s1action2 simulation. Proteins are represented by ribbon diagrams and stick models with nitrogen atoms in dark blue, oxygen in red, sulfur in yellow orange and carbon in salmon color (SNARE complex) or green (Syt1 C<sub>2</sub>B domain). Acidic residues from the SNAREs and the three arginines of the C<sub>2</sub>B domain are labeled. R59 of SNAP-25 is also labeled, as it may affect the interactions between C<sub>2</sub>B arginines and SNARE acidic residues.

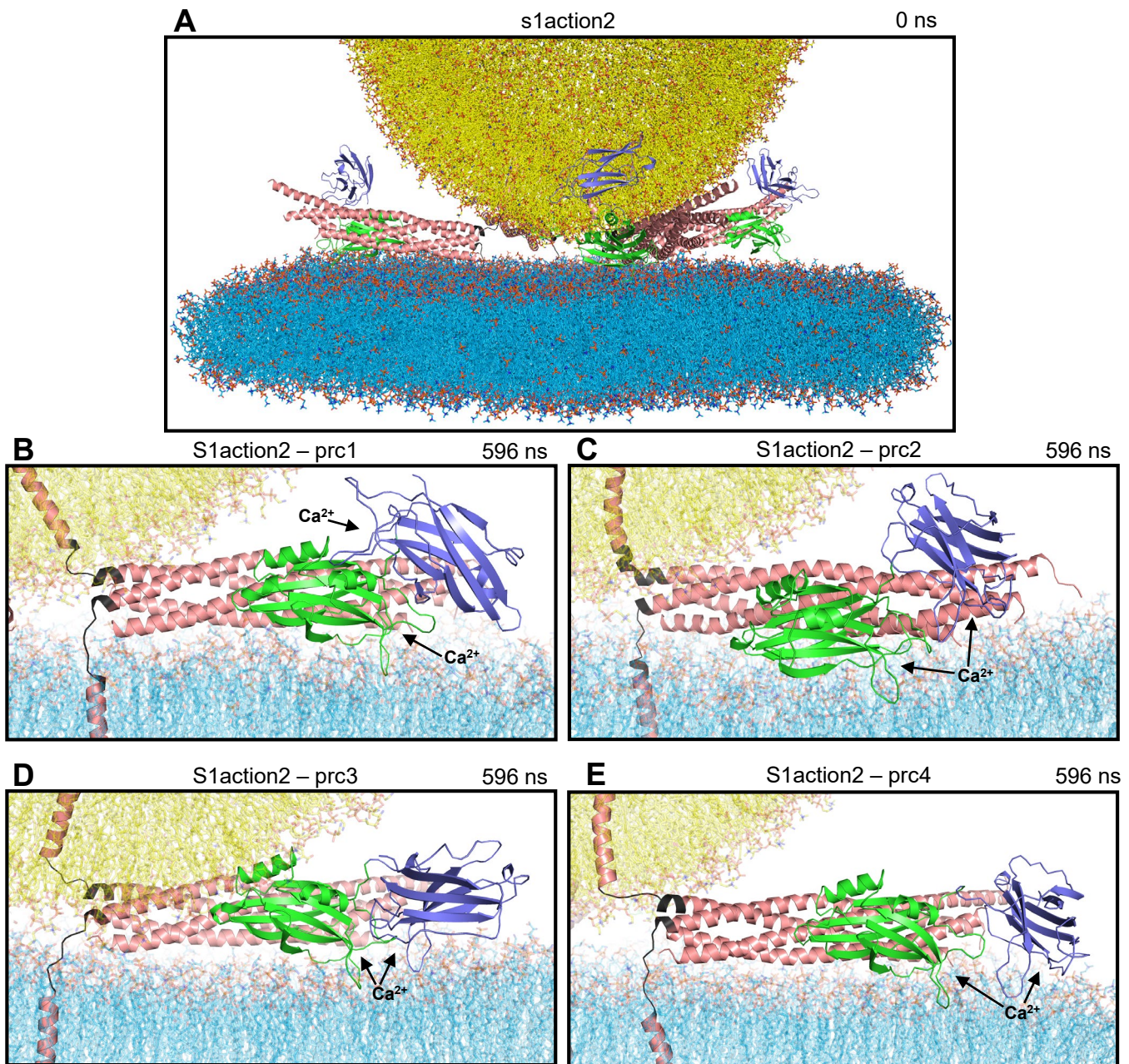


**Figure S18.** MD simulation of primed Syt1 C<sub>2</sub>AB-SNARE complexes bridging a vesicle and a flat bilayer (s1action2 simulation). (A) Initial configuration of the system. (B-E) Close-up views of the four primed complexes (prc1-prc4) after 596 ns of MD simulation. The arrows point at the Ca<sup>2+</sup>-binding sites of the C<sub>2</sub>A and C<sub>2</sub>B domains. Lipids are represented by stick models and proteins by ribbon diagrams with the same color coding as in Fig. 1, except that the jxt linkers of synaptobrevin and syntaxin-1 are colored in dark gray. Note the similarity of the orientations of the C<sub>2</sub>B domain with respect to the SNARE complex and the flat bilayer for the different complexes, the different conformations adopted by the jxt linkers, and the different locations of the C<sub>2</sub>A domain, although in three complexes (prc2-prc4) the Ca<sup>2+</sup>-binding loops of the C<sub>2</sub>A domain are located close to those of the C<sub>2</sub>B domain, which can facilitate a cooperative action of both domains.

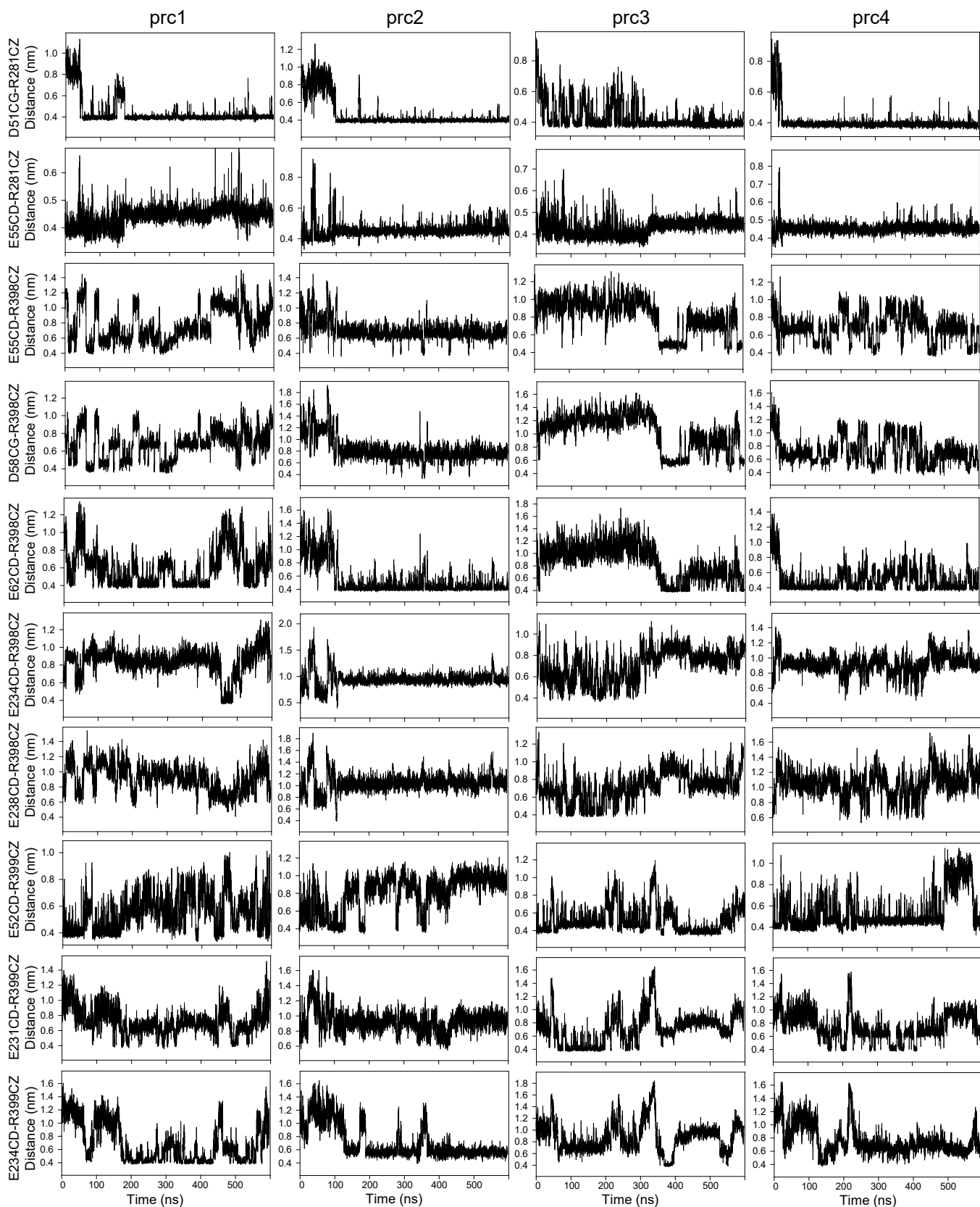


**Figure S19.** Distances between Syt1 C<sub>2</sub>B domain arginines and SNARE acidic residues at region II of the primary interface during the s1action2 MD simulation. The time dependence (0.1 ns steps) of the distances indicated at the y axes is shown for the four complexes (prc1-prc4) of the simulation.



S1action2 – prc2

596 ns

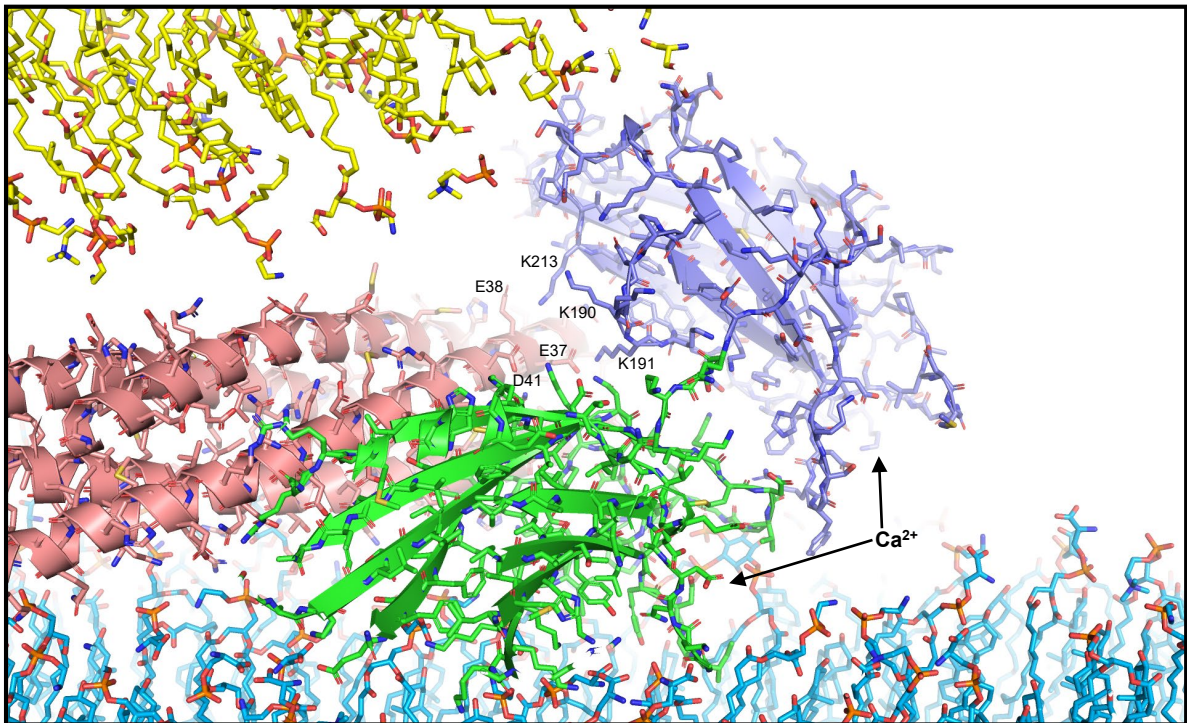


**Figure S20.** Close-up view of one of the primed complexes (prc4) of the s1action2 MD simulation at 596 ns. Lipids are represented by stick models and proteins by ribbon diagrams and stick models with the same color coding as in Fig. 1 and 2. Basic residues of the C<sub>2</sub>A domain that are close to an acidic patch of the SNARE complex are labeled. The arrows indicated the Ca<sup>2+</sup>-binding sites of the two C<sub>2</sub> domains.

## SI References

1. W. Kuo, D. Z. Herrick, D. S. Cafiso, Phosphatidylinositol 4,5-bisphosphate alters synaptotagmin 1 membrane docking and drives opposing bilayers closer together. *Biochemistry* **50**, 2633-2641 (2011).
2. R. Voleti, K. Jaczynska, J. Rizo, Ca(2+)-dependent release of Synaptotagmin-1 from the SNARE complex on phosphatidylinositol 4,5-bisphosphate-containing membranes. *Elife* **9**, e57154 (2020).
3. J. S. Rhee *et al.*, Augmenting neurotransmitter release by enhancing the apparent Ca<sup>2+</sup> affinity of synaptotagmin 1. *Proc. Natl. Acad. Sci. U. S. A* **102**, 18664-18669 (2005).
4. M. Ruiter *et al.*, An Electrostatic Energy Barrier for SNARE-Dependent Spontaneous and Evoked Synaptic Transmission. *Cell Rep* **26**, 2340-2352 e2345 (2019).
5. R. Mohrmann, W. H. de, M. Verhage, E. Neher, J. B. Sorensen, Fast vesicle fusion in living cells requires at least three SNARE complexes. *Science* **330**, 502-505 (2010).
6. D. Van Der Spoel *et al.*, GROMACS: fast, flexible, and free. *J Comput Chem* **26**, 1701-1718 (2005).
7. S. Pronk *et al.*, GROMACS 4.5: a high-throughput and highly parallel open source molecular simulation toolkit. *Bioinformatics* **29**, 845-854 (2013).
8. R. B. Best *et al.*, Optimization of the additive CHARMM all-atom protein force field targeting improved sampling of the backbone phi, psi and side-chain chi(1) and chi(2) dihedral angles. *J Chem Theory Comput* **8**, 3257-3273 (2012).
9. J. Rizo, L. Sari, K. Jaczynska, C. Rosenmund, M. M. Lin, Molecular mechanism underlying SNARE-mediated membrane fusion enlightened by all-atom molecular dynamics simulations. *Proc Natl Acad Sci U S A* **121**, e2321447121 (2024).
10. J. Rizo, L. Sari, Y. Qi, W. Im, M. M. Lin, All-atom molecular dynamics simulations of Synaptotagmin-SNARE-complexin complexes bridging a vesicle and a flat lipid bilayer. *Elife* **11**, e76356 (2022).
11. S. Takamori *et al.*, Molecular anatomy of a trafficking organelle. *Cell* **127**, 831-846 (2006).
12. R. B. Chan *et al.*, Comparative lipidomic analysis of mouse and human brain with Alzheimer disease. *J Biol Chem* **287**, 2678-2688 (2012).
13. J. Ubach, X. Zhang, X. Shao, T. C. Sudhof, J. Rizo, Ca<sup>2+</sup> binding to synaptotagmin: how many Ca<sup>2+</sup> ions bind to the tip of a C2-domain? *EMBO J* **17**, 3921-3930 (1998).
14. I. Fernandez *et al.*, Three-dimensional structure of the synaptotagmin 1 c(2)b-domain. Synaptotagmin 1 as a phospholipid binding machine. *Neuron* **32**, 1057-1069 (2001).
15. J. Rizo *et al.*, Conformational-Analysis of A Highly Potent, Constrained Gonadotropin-Releasing-Hormone Antagonist .1. Nuclear-Magnetic-Resonance. *Journal of the American Chemical Society* **114**, 2852-2859 (1992).
16. J. Rizo *et al.*, Conformational-Analysis of A Highly Potent, Constrained Gonadotropin-Releasing-Hormone Antagonist .2. Molecular-Dynamics Simulations. *Journal of the American Chemical Society* **114**, 2860-2871 (1992).
17. J. Rizo, L. M. Gierasch, Constrained peptides: models of bioactive peptides and protein substructures. *Annu. Rev. Biochem* **61**, 387-418 (1992).
18. Y. V. Grinkova, I. G. Denisov, S. G. Sligar, Engineering extended membrane scaffold proteins for self-assembly of soluble nanoscale lipid bilayers. *Protein Eng Des Sel* **23**, 843-848 (2010).
19. E. A. Prinslow, K. P. Stepien, Y. Z. Pan, J. Xu, J. Rizo, Multiple factors maintain assembled trans-SNARE complexes in the presence of NSF and alphaSNAP. *Elife* **8**, e38880 (2019).
20. Q. Zhou *et al.*, Architecture of the synaptotagmin-SNARE machinery for neuronal exocytosis. *Nature* **525**, 62-67 (2015).
21. K. Jaczynska *et al.*, Analysis of tripartite Synaptotagmin-1-SNARE-complexin-1 complexes in solution. *FEBS Open Bio* **13**, 26-50 (2023).

22. A. Zhou, K. D. Brewer, J. Rizo, Analysis of SNARE complex/synaptotagmin-1 interactions by one-dimensional NMR spectroscopy. *Biochemistry* **52**, 3446-3456 (2013).
23. Parrinello M, Rahman A. 1981. Polymorphic transitions in single crystals: A new molecular dynamics method. *Journal of Applied Physics* **52**:7182–7190
24. Hoover T. 1985. Canonical dynamics: Equilibrium phase-space distributions. *Physical Review. A, General Physics* **31**:1695–1697.
25. Darden T, York D, Pedersen L. 1993. Particle mesh Ewald: an N·log(N) method for Ewald sums in large systems. *The Journal of Chemical Physics* **98**:10089–10092.